# Chapter 2
# Solar Radiation in Forests: Theory for Hemispherical Photography

**Patrick Schleppi and Alain Paquette**

**Abstract** Solar radiation is not only the main source of energy for life on Earth, but it is also the natural source of light for the optical acquisition of information, such as for vision and photography. Natural sunlight provides the illumination required for taking hemispherical photographs in forests. In turn, such photographs can then be interpreted to provide a description of the plant canopy and its interactions with light, or more generally, its radiation regime. The techniques used for both the acquisition and the analysis of hemispherical photographs are based on the theory of radiation in plant canopies. The goal of this chapter is to present the theoretical foundations describing how solar radiation reaches Earth's surface and interacts with plant canopies. Different sensors for measuring radiation are described, and the principles of hemispherical photography are reviewed. Finally, a comparison of the techniques used to assess the radiation regime of forest canopies is presented.

**Keywords** Energy budget · Forest canopy · Light sensor · Solar radiation · Overcast sky models · Atmospheric effects

## 2.1 Introduction

Hemispherical photography (HP) consists of taking pictures in an upward direction through an extreme wide-angle lens (i.e., a lens having a field of view close to 180°) (Rich 1990). By accounting for the geometry of light transmission and interception,

P. Schleppi (✉)
Swiss Federal Institute for Forest, Snow and Landscape Research (WSL),
Zürcherstr. 111, 8903 Birmensdorf, Switzerland
e-mail: schleppi@wsl.ch

A. Paquette
Centre for Forest Research, Université du Québec à Montréal (UQAM),
P.O. Box 8888 Centre-Ville Station, Montréal, QC H3C 3P8, Canada
e-mail: alain.paquette@gmail.com



R.A. Fournier and R.J. Hall (eds.), *Hemispherical Photography in Forest Science: Theory, Methods, Applications*, Managing Forest Ecosystems 28,
DOI 10.1007/978-94-024-1098-3_2

HP has been successfully used to characterize the structure of forest canopies and the radiation regime of forests. The interpretation of hemispherical photographs is based on theoretical assumptions concerning the interactions between light and the canopy. Conversely, ecosystem modeling requires empirical information on the quantity of foliage, the structure of the canopy, and the properties of incoming solar radiation (e.g., Running and Coughlan 1988). Understanding these patterns and processes is necessary for the correct application and interpretation of HP. Our objective in this chapter is to provide the reader with an introduction to solar radiation in forests with an emphasis on HP.

The Sun is the main source of radiation on Earth; for this reason, we first review the basic physics of solar radiation and its interactions with the atmosphere. Second, we examine the interactions between radiation and forest canopies, which are the main processes that HP aims to describe. Third, we present different types of radiation sensors and discuss their main applications, especially in relation to HP. Last, we briefly discuss the strengths and limitations of HP for assessing forest canopies and their radiation regimes.

## 2.2 Solar Radiation

Solar radiation, the electromagnetic energy that originates from the Sun, is the essential source of energy that drives climate and life processes on Earth (Gates 1980). In forests, solar radiation is important for diverse biological and physical processes such as photosynthesis, growth, carbon cycling, evapotranspiration, and temperature regimes. In spite of this essential role, solar radiation has received less attention compared to other meteorological parameters such as temperature, precipitation and wind. This disparity can be explained, in part, by the difficulties of measuring radiation. Furthermore, while other meteorological factors can lead to accidents or disasters (e.g., frosts, droughts, floods, windstorms), solar radiation always remains within a range to which ecosystems are adapted, thus making it "good-natured" and easily forgotten. Nevertheless, foresters and ecologists have long recognized that differences exist among species regarding their tolerance to shade (e.g., Engler 1924). While shade-intolerant species are typically pioneer trees, shade-tolerant species appear later in succession because they can grow under denser canopies or at least survive until a gap opens above them. The degree of shade-tolerance of shrubs, herbaceous species, and mosses is also important in determining their occurrence in forests. A favorable light regime is important for tree establishment; therefore, optimizing light availability for seedlings is an important objective for forest management practices, especially in uneven-aged stands and in mixed forests (Lieffers et al. 1999; Drever and Lertzman 2003; Paquette et al. 2006). Here, we provide an introduction to this subject by examining how solar radiation varies in time and space. Numerous textbooks describe the influence of solar radiation on the Earth; for example, Bohren and Clothiaux (2006) and Timofeyev and Vasil'ev (2008) provide reviews covering the physical concepts

that are presented in this chapter. The Sun's radiation is maximal around a wavelength of 500 nm (Fig. 2.1). According to Wien's law, this corresponds to a temperature of nearly 5800 K for the light-emitting layer (i.e., the photosphere). The emission of solar radiation covers the whole spectrum that is visible to the human eye (380–750 nm) and extends into the ultraviolet and near-infrared bands. This spectrum is often referred to as shortwave radiation. In contrast, longwave infrared radiation is emitted by surfaces at near-ambient temperatures. By definition, the boundary between shortwave and longwave radiation is set at 4000 nm.

When solar radiation reaches Earth's upper atmosphere, it delivers an average power of 1367 W $m^{-2}$ when measured perpendicularly to the Sun's rays. This "solar constant" varies by a few W $m^{-2}$, depending upon the amount of solar activity during a solar cycle. Stronger variations occur due to the eccentricity of the Earth's orbit (Fig. 2.2) because radiation flux is inversely proportional to the squared distance between the source and target (i.e., between the Sun and Earth). The effect of orbital eccentricity on the solar constant is given by

$$E_o = (r_o/r)^2 = 1.00011 + 0.03423\cos\Gamma + 0.00092\sin\Gamma + 0.00072\cos 2\Gamma + 0.00006\sin 2\Gamma \quad (2.1)$$

with

$$\Gamma = 2\pi d/365.25, \quad (2.2)$$

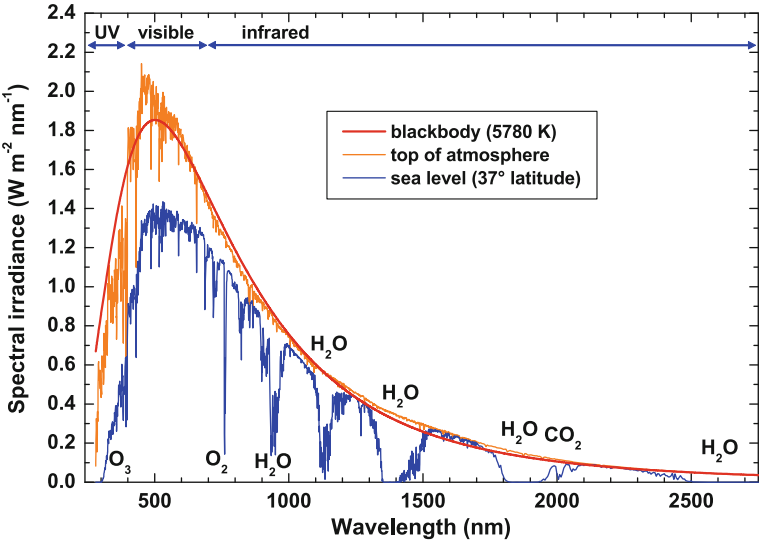


**Fig. 2.1** Solar radiation spectrum at the top of Earth's atmosphere and at sea level for direct radiation. Emission of a black body after Planck's law. The main absorption bands of atmospheric gases are indicated by their chemical formulas. *Data source* Emery and Myers (2008)

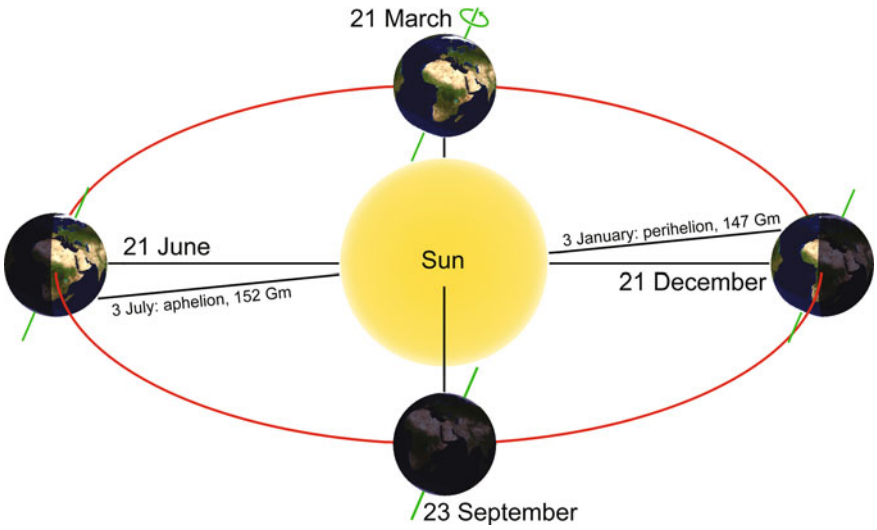


**Fig. 2.2** Scheme of Earth's rotation around the Sun, showing the declination of Earth's axis that explains the seasons

where $r_o$ is the average distance and $r$ is the current distance to the Sun. The term $\Gamma$ is referred to as the day angle and $d$ is the number of days since 12:00 UTC (Coordinated Universal Time), 1 January of the last intercalary or leap year. In addition to precession, long-term changes occur in eccentricity and obliquity, together with long-term changes in solar activity. According to the theory of Milankovitch (1941), these effects (which are amplified by feedbacks involving Earth's albedo) are responsible for the ice age cycles of the last few million years. Such long-term variations will not be developed here.

Because the total area of a sphere is four times its cross-section (i.e., its projected area), the average incoming radiation at the top of the atmosphere is 1367/4 = 342 W $m^{-2}$ when measured horizontally. Its value varies between 0 for Earth's nighttime hemisphere and the solar constant for the subsolar point, which is the location within the tropics where the Sun is directly overhead (i.e., in zenith). Averaged over a year, solar radiation $I_0$ at the top of the atmosphere is about 417 W $m^{-2}$ at the equator and 173 W $m^{-2}$ at the poles, or

$$I_0 = I_s(0.219 + 0.092\cos 2\Phi - 0.005\cos 4\Phi - 0.002\cos 6\Phi + 0.002\cos 8\Phi) \tag{2.3}$$

where $\Phi$ is the latitude and $I_s$ is the solar constant. Note that in spite of Earth's orbital eccentricity, this relationship is practically identical for the southern and northern hemispheres of our planet. This is because the length of the seasons (longer summer in the northern hemisphere) compensates for differences in radiation (shorter Sun-Earth distance when it is summer in the southern hemisphere).

The position of the Sun in the sky can be plotted on a sky map showing the daily sun tracks over the course of a year. Such a map has a geometry that is similar to a hemispherical photograph, where the zenith and azimuth angles are presented as polar coordinates. A map of sun tracks can be combined with a hemispherical photograph, which is used as a mask in order to show the potential duration of direct radiation at the point where the photograph was taken. In a forest, this information is especially useful for characterizing the prevailing under-canopy light regime for the ground vegetation, including tree recruitment. This simple approach, however, does not take into account atmospheric effects, which is the topic of the next section.

## 2.3 Atmospheric Absorption and Scattering

Solar radiation is partly absorbed by gas molecules, mainly triatomic compounds, in traveling through the atmosphere. Water vapor ($H_2O$) and carbon dioxide ($CO_2$) primarily absorb energy in the infrared band, while ozone ($O_3$) absorbs in the ultraviolet (Fig. 2.1). Solar radiation is further absorbed and scattered by other gases, aerosol particles, and clouds. Very small-diameter particles, which are much smaller than the wavelength of light, or microscopic fluctuations in air density can cause Rayleigh scattering. Blue light is scattered more than other visible colors due to its shorter wavelength. The blue color of a clear sky is due to diffuse sky radiation resulting from Rayleigh scattering of sunlight in the atmosphere. When the Sun is low on the horizon, the missing blue light that has been scattered away leaves the direct sunlight with an orangish or reddish color. The angle between the original and scattered radiation is the scattering angle. In Rayleigh scattering, this angle has a statistical distribution that is maximal at 0 and $\pi$ rad; in other words, scattered radiation is preferentially directed forward or backward as opposed to the sideward directions. Aerosol particles with diameters of the same order of magnitude as the wavelength of radiation produce Mie scattering. In contrast to Rayleigh scattering, the Mie scattering pattern is relatively independent of wavelength and is preferentially in a forward direction.

Solar radiation also interacts with ice crystals and water droplets in clouds. Multiple reflections and refractions cause scattering. Statistically, all wavelengths diffuse similarly, resulting in the whitish or grayish color of clouds. However, some separation of wavelengths occurs when the number of refractions and reflections is small. This is the case for rainbows, where sunlight is refracted when entering a water droplet, reflected inside, and refracted again upon exiting (or two reflections for a secondary rainbow).

Because much of the solar radiation is scattered back into space by air and clouds, only a fraction of it reaches Earth's surface. The atmosphere affects incoming solar radiation according to the following proportions (Timofeyev and Vasil'ev 2008):

26% is absorbed and heats the stratosphere and thermosphere,
24% is scattered back by the atmosphere and is reflected to space,

22% is scattered and reaches Earth's surface as diffuse radiation,
28% is transmitted and reaches Earth's surface as direct radiation.

Together with corresponding values for near- and longwave infrared radiation, these numbers determine Earth's radiative balance and its average temperature. Direct radiation dominates under clear skies, but it can be completely blocked by clouds that only allow diffuse radiation to pass through. For example, direct radiation dominates over deserts. Over most forests of the world, direct and diffuse radiation roughly contribute equally to global radiation on an annual basis. However, direct radiation is more variable over time and space compared to diffuse radiation because the former is more dependent upon the season, time of day, topography, and weather. In meteorology and climatology, various atmospheric radiative transfer models have been developed to take into account the effects of weather conditions; these are the so-called atmospheric radiative transfer codes.

For a particular time and point on Earth, the transmission (or transmittance, a dimensionless ratio) of radiation through a cloudless atmosphere can be described by the Beer-Lambert-Bouguer law as a function of the atmospheric thickness along the path that the radiation is traveling. Transmission depends on the elevation of the Sun (i.e., the angle between the Sun and horizon, see Eq. 2.13 below for its calculation). The transmittance $T$ is given by

$$T = \tau^{p/p_0 \sin\beta} = \tau^{p/p_0 \cos\theta} = \mathrm{e}^{-kp/p_0 \cos\theta}, \tag{2.4}$$

where $\tau$ is transmittance at normal pressure ($p_0$ = 1013 hPa), $p$ is local air pressure, $\beta$ is the elevation of the Sun above the horizon, and $\theta$ is its zenith angle ($\beta$ + = 90° = $\pi$/2 rad). The absorption coefficient is defined as $k = -\ln \tau$, which can be considered as the sum of the absorption coefficients of the different atmospheric constituents (i.e., gases and aerosols). Air pressure is used here as a measure of the air mass above the point of interest, which is referred to as the optical mass of the atmosphere. At higher altitudes, the pressure is lower and the corresponding transmission is higher.

At Sun elevations below 5° (or 0.1 rad), some refraction occurs and the Sun appears to be slightly higher in the sky than it really is. At the same time, the path of sunlight through the atmosphere is shortened because of the latter's curvature. These effects can be approximated by

$$T = \tau^{p/p_0 \cos(0.99\theta)} = \mathrm{e}^{-kp/p_0 \cos(0.99\theta)} \tag{2.5}$$

The Beer-Lambert-Bouguer law is essentially valid for any wavelength or spectral band but with variable absorption coefficients. For a clear atmosphere, $\tau$ is close to 0.8 for visible light, but this value can be affected by air pollution (Jacobson 2002).

Local measurements that have been made consecutively over years are necessary to obtain reliable estimates of the true transparency of the atmosphere and its variation by taking both direct and diffuse radiation into account. Where sunlight

duration is available but no radiation measurements have been made, it is possible to estimate the latter by regional adaptation of an Angström-Prescott model (Angström 1924; Prescott 1940), such that

$$T = a + b(D/D_0) + c(D/D_0)^2. \tag{2.6}$$

Equation 2.6 is the quadratic or second-order model; the linear or first-order model would have $c = 0$. The variable $D$ is the measured duration of sunlight (often calculated per month) and $D_0$ is the maximal duration without any cloudiness. Estimates of the regression parameters (i.e., $a$, $b$ and $c$) are available for many regions of the world and there is a large body of corresponding technical publications from studies on solar energy. In a recent review, Akinoglu (2008) gives the following ranges for the linear model: $0.06 \leq a \leq 0.46$ and $0.19 \leq b \leq 0.87$. The value of $D_0$ is obtained by calculating the hour angle at sunrise and sunset. The difference is transformed from an angle into a duration, such that

$$\cos \omega_1 = \cos \omega_2 = -\tan \Phi \tan \delta, \tag{2.7}$$

where $\Phi$ is the latitude, and $\delta$ is the declination of the Sun. The respective hour angles at sunrise and sunset are $\omega_1$ and $\omega_2$, where the first term is the negative arccosine and the second term is the positive arccosine. Because they are approximately symmetrical around $\omega = 0$ (solar noon), the day length is $2\omega_2$; in hours it is

$$D_0 = 24\omega_2/\pi = 24 \arccos(-\tan \Phi \tan \delta)/\pi \tag{2.8}$$

Note that no solutions are found if the Sun remains either above or below the horizon. In these cases, $D_0 = 24$ or $D_0 = 0$, referring to midnight sun and polar night, respectively. The declination δ is the angle between Earth's orbit around the Sun (i.e., orbital plane) and Earth's equator (i.e., equatorial plane). It varies with the season between −23.45° (−0.409 rad) at the December solstice and +23.45° (+0.409 rad) at the June solstice. It can be calculated (in rad) approximately as

$$\delta = -0.409 \cos[2\pi/365(d + 10)], \tag{2.9}$$

where $d$ is the day of the year. A more precise formula takes the eccentricity of Earth's orbit into account (Spencer 1971). We recalculated Spencer's coefficients also to take into account leap years (via Eq. 2.2 for the calculation of $\Gamma$), and optimized them for the years 2011–2030. From this development, declination can be calculated as

$$\begin{aligned}\delta = {} & 0.006918 - 0.399912 \cos \Gamma + 0.070257 \sin \Gamma - 0.006758 \cos 2\Gamma \\ & + 0.000907 \sin 2\Gamma - 0.002697 \cos 3\Gamma + 0.00148 \sin 3\Gamma,\end{aligned} \tag{2.10}$$

with a standard deviation (SD) of 0.00025 rad (0.014°), compared to 0.017 rad (1°) for Eq. 2.9. Angström-Prescott models were developed from an intuitive

point-of-view using statistical methods. A theoretical basis for these models was recently proposed by Pelkowski (2008). A three-layer atmospheric model is used, where a layer containing clouds is sandwiched between two clear layers. The radiation fluxes in two streams (i.e., direct and diffuse) were modeled through these layers, including reflection from Earth's surface. Pelkowski (2008) concluded that an Angström-Prescott polynomial is a valid approximation and it should generally be at least of a second-order form.

In this section, we have examined how the atmosphere quantitatively affects the radiation traversing it. For most applications, including HP, we also need to consider the angles between the radiation and the objects interacting with it on Earth, which is the topic of the next section.

## 2.4 Geometry of Solar Radiation on Earth's Surface

The radiative power that is received by a flat surface is maximal when it directly faces the source, i.e., when the angle of incidence is 0. When radiation is parallel to the surface, it delivers no energy. Between these extremes, Lambert's Cosine law applies (Fig. 2.3), such that the radiative flux $I$ onto the surface area is given by

$$I = I_0 \cos\gamma = E_o I_s T \cos\gamma, \tag{2.11}$$

where $I_0$ is the incident flux (measured perpendicularly), and $\gamma$ is the angle of incidence. The term $I_s$ is the solar constant, $E_o$ is the correction for the eccentricity of Earth's orbit, and $T$ is the transmittance of the atmosphere. On flat ground, the angle of incidence is equal to the zenith angle, but this is not the case on a slope.

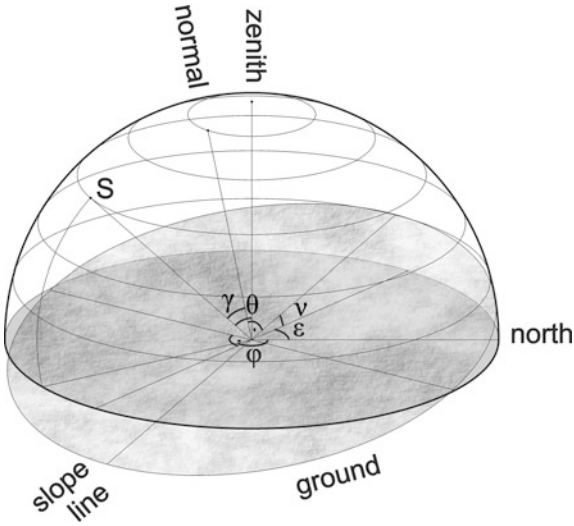


**Fig. 2.3** Geometry of solar radiation on an inclined surface. S = position of the Sun in the sky, θ = its zenith angle, $\varphi$ = its azimuth, ν = slope angle, ε = aspect (orientation of the slope), γ = angle of incidence of the direct radiation on the ground

For sunlight, $\gamma$ is taken through the center of the Sun. Strictly speaking, it should be integrated over the apparent sun disk, which covers an angle of about 0.009 rad (or slightly more than 0.5°). As long as the Sun is entirely visible, using only the angle through the center results in a negligible source of error. The power delivered by direct solar radiation onto a slope is calculated by

$$\cos\gamma = \sin\beta\cos v + \cos\beta\cos(\varepsilon - \varphi)\sin v, \tag{2.12}$$

where $\beta$ is the elevation of the Sun, $\varphi$ is its azimuth, $v$ is the slope angle, and $\varepsilon$ is the aspect (i.e., orientation of the slope).

To calculate the position of the Sun, it is necessary to know the local coordinates upon Earth's surface and the time, such that

$$\sin\beta = \cos\theta = \sin\Phi\sin\delta + \cos\Phi\cos\delta\cos\omega \tag{2.13}$$

and

$$\cos\varphi = (\cos\Phi\sin\delta - \sin\Phi\cos\delta\cos\omega)/\cos\beta, \tag{2.14}$$

where $\Phi$ is the latitude, and $\delta$ is the declination of the Sun. Taking the arccosine from Eq. 2.14 yields two alternate solutions, one valid for the morning ($\omega < 0$ $0 < \varphi < \pi$) and the other for the afternoon ($\omega > 0 \Rightarrow \pi < \varphi < 2\pi$). The hour angle $\omega$ is the local solar time expressed as an angle instead of hours, minutes, and seconds; a value of zero indicates solar noon. The hour angle is calculated as

$$\omega = (t - 12)\pi/12 - \lambda - \Delta\omega \tag{2.15}$$

with

$$\Delta\omega = 0.0002\cos\Gamma - 0.0335\sin\Gamma - 0.0159\cos 2\Gamma - 0.0400\sin 2\Gamma, \tag{2.16}$$

where $\lambda$ is the longitude, $t$ is the UTC (Coordinated Universal Time) in hours, and $\Delta\omega$ is the equation for time, i.e., the difference between true solar time and average solar time, expressed here as an angle. This difference arises from the obliquity of Earth's axis and from the eccentricity of its orbit. The term $\Delta\omega$ varies roughly by $\pm 0.07$ rad, equivalent to $\pm$¼ h, with two minima and two maxima over the year. (See Eq. 2.2 for the calculation of $\Gamma$.) Given this formula, $\omega$ is obtained in rad. Note that the equation for time is defined with the opposite sign in some countries, such as France.

When Eqs. 2.11–2.14 are combined and the expressions are rearranged, they yield Iqbal's formula (Iqbal 1983), such that

$$\begin{aligned} I = E_o I_s T\big(&(\sin\Phi\cos v - \cos\Phi\sin v\cos\varepsilon)\sin\delta \\ &+ (\cos\Phi\cos v + \sin\Phi\sin v\cos\varepsilon)\cos\delta\cos\omega \\ &+ \cos\delta\sin v\sin\varepsilon\sin\omega\big). \end{aligned} \tag{2.17}$$

This formula is deterministic except for its $T$ term: atmospheric transmission is indeed subject to stochastic weather conditions. If certain restrictions or assumptions are applied to $T$ (e.g., considering only clear skies or average overcast conditions), then the equation can be integrated numerically over time to obtain the average direct radiation. Using $\tau = 0.8$ in Eq. 2.5, we calculated yearly values over a large range of latitudes (−72° to 72°) and slopes (0° to 60°), and for all aspects. We subjected the results to multiple regression and, consequently, yearly average radiation under a clear sky $I_a$ can be approximated as

$$\begin{aligned} I_a = I_s(&0.0631 + 0.1964(\cos \Phi)^2 \cos v \\ &- 0.1063 \sin v \cos \varepsilon \sin 2\Phi - 0.0238 \cos \Phi \cos 2\Phi \\ &- 0.0117 \sin v \cos \Phi \cos 2\varepsilon). \end{aligned} \tag{2.18}$$

The coefficient of determination is $R^2 = 0.998$, and the precision of the integration is 0.4% (results not previously published). This formula covers almost all forests of the world, but it only takes a single slope into account rather than considering complex topography that would modify the radiation, such as the opposing slope of a valley.

The geometry of diffuse radiation is important for its interaction with tilted surfaces or with complex structures such as a plant canopy (see review by Torres and Torres 2008). This geometry can be described separately for clear and overcast skies. Diffusion in clear air and in clouds produces different patterns of radiance (i.e., radiation per unit of solid angle) and, consequently, different colors. In a clear sky, photons are not scattered in all directions but preferentially travel forward. Radiance is thus anisotropic (Brunger and Hooper 1993): it is higher near the Sun and decreases with the scattering angle. The pattern of this decrease depends upon the relative importance of Rayleigh and Mie scattering; in other words, it varies with the turbidity of the atmosphere (e.g., Vida et al. 1999). Some models also account for the effect of zenith angle since it is related to the optical mass of the atmosphere (Hooper and Brunger 1980; Harrison and Coombes 1988). Because scattering is a function of wavelength, different parameters have to be used in the model, depending upon which band of the spectrum is being considered. For example, scattering of near-infrared radiation is not the same as scattering of photosynthetically active radiation (PAR).

Under a uniformly overcast sky where the Sun is not visible, a first approximation considers the clouds as a diffusive horizontal surface with radiance subjected to Lambert's Cosine law. This results in isotropic radiance (i.e., radiance with the same value over the whole visible sky). This model is referred to as "uniform overcast sky" (UOC). Consideration of the thickness of clouds and reflections between clouds and Earth's surface leads to a model referred to as a "standard overcast sky" (SOC) in which radiance is a function of the zenith angle θ (Steven and Unsworth 1980), such that

$$I(\theta) = I(0)(1 + b\cos\theta)/(1 + b), \tag{2.19}$$

where $b$ is an empirically determined factor, typically between 0.5 and 1.5. On a slope $v$, total radiation is reduced compared to a flat surface because part of the sky is obstructed (Steven and Unsworth 1980), such that

$$I = I_0(\cos v/2)^2 + 2b\left[\sin v - v\cos v - \pi(\sin v/2)^2\right]/[\pi(3 + 2b)]. \tag{2.20}$$

Since the UOC model corresponds to $b$ = 0, the effect of slope simplifies in that case to the factor $(\cos v/2)^2$.

There are also models that describe partly overcast skies where the Sun is visible through uniform clouds (Hooper and Brunger 1980; Grant et al. 1996). Such models combine a distribution function that is based on theory with parameters that are fitted empirically. Like the Angström-Prescott polynomials that were discussed in the previous section, these models have regional validity and need to be adapted to different climatic conditions (Siala and Hooper 1990). An additional model describes luminance, which is the brightness of light that is emitted or reflected from a surface as perceived by the human eye, which is more sensitive to green than to red and blue wavelengths. In this model (Kittler 1994; CIE 2003), luminance is characterized as combining a function of the zenith angle ("gradation") and a function of the scattering angle ("indicatrix"). For each of these functions, standard parameter sets are provided to match most typical situations ranging between clear and overcast skies. This model was developed primarily for industrial and architectural lighting applications, but it can also be adapted to environmental radiance measurements, viz., the analysis of hemispherical images (Lang et al. 2010). The method consists of using a radiance model to interpolate between sky patches that are visible through canopy openings so as to obtain a virtual reference image. Image analysis is then performed by comparing the actual hemispherical photograph with the interpolated reference.

On a slope, the same geometrical rules apply as for direct radiation, with the difference being that they have to be integrated over all sky directions, which means a double integration over the zenith and azimuth angles. Liu and Jordan (1961) have provided an integrated formula based on isotropic diffusion and isotropic reflection by the surrounding ground. Hay's model (Hay and McKay 1985) is similar but is based on anisotropic diffusion. In complex terrain, the integration of diffuse sky radiation is obviously limited to the visible portion of the sky (e.g., Wang et al. 2005), but reflection from surrounding slopes may also have to be considered. Like the case of sun tracks being combined with a hemispherical photograph to derive potential direct radiation (see Sect. 2.2), a model of sky radiation can be used to calculate diffuse radiation that is transmitted by the pictured canopy and to integrate it over time. There is, however, more information about the structure of the canopy to be gained from a hemispherical photograph than just creating a sky mask. In the next section, the theoretical background for the extraction of this information will be examined.

## 2.5 Interactions of Solar Radiation with Forest Canopies

In the preceding sections, we have considered how much solar radiation reaches a given surface on Earth. Compared to a solar panel, a forest canopy has a complex geometry with receptors (the leaves) that do not all face the same direction and are not all exposed to direct radiation. Their power yields (photosynthesis) and maintenance costs (transpiration and respiration) are thus highly variable in time and space, and much more difficult to predict than the output of a solar panel. Except in cases when the gas exchange of a single leaf is measured under known light conditions, it is necessary to consider that radiation is heterogeneous within the canopy and that photosynthesis shows a non-linear response to irradiance (e.g., Sinclair et al. 1976). Photosynthesis is further limited by the radiation spectrum that it can use. Since they both evolved under the same radiation spectrum, photosynthesis in terrestrial plants and human vision cover about the same spectrum. By definition, photosynthetically active radiation (PAR) is the band of wavelengths that ranges from 400 to 700 nm. Blue and red light are preferentially absorbed by photosynthetic pigments, while green light tends to be reflected, giving leaves their characteristic color (Fig. 2.4).

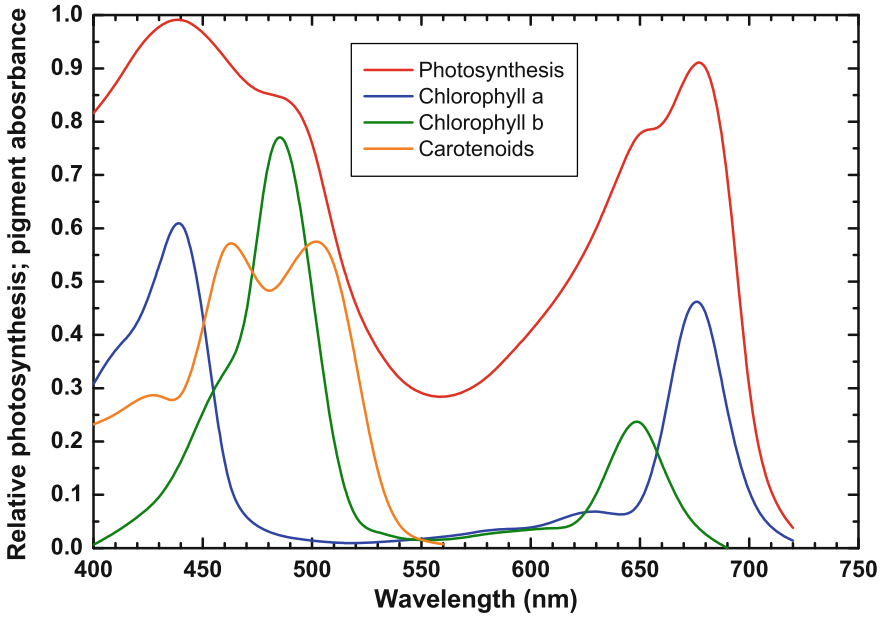


**Fig. 2.4** Absorption spectra of photosynthetic pigments and photosynthesis rate as a function of wavelength. Redrawn from Singhal et al. (1999) and Lodish et al. (2000)

### 2.5.1 Canopy Radiation Models

Absorption, scattering, and transmission modify radiation as it interacts with a leaf or with a plant canopy (Fig. 2.5). The intensity, the spectral distribution, and the ratio of direct-to-diffuse radiation are all affected by these interactions. At the level of single leaves, several dimensionless coefficients can be defined as follows: absorbance, $\alpha = A/I$; reflectance, $\rho = R/I$; and transmittance, $\tau = (T + S)/I$ (see Fig. 2.5 for abbreviations). Note that, depending upon the application, transmission can refer either to $T$ or to $T + S$. To distinguish between these two terms, $T + S$ is sometimes called non-interceptance. Radiation scattering is summarized as a scattering coefficient $\omega = (R + S)/I$ (here, the symbol $\omega$ is different from the solar hour angle $\omega$ in Eqs. 2.7–2.17). For a leaf, transmission without scattering is very small and, thus, $\omega \approx \tau + \rho = 1 - \alpha$. A typical spectrum for leaves is shown in Fig. 2.6. It can be seen that absorption dominates in the visible range, while scattering (reflection and transmission) dominates in the near-. The amount of radiation that is absorbed or scattered by a leaf also depends upon the angle of incidence, which determines the projected leaf area in the direction of the radiation. Individual leaves are not always flat and their inclination angle within a canopy is not constant but displays a statistical probability distribution. Several models have been proposed to describe this probability distribution; the most common ones include the ellipsoidal distribution, beta distribution, de Wit's function, and the Ross-Goudriaan function (see Wang et al. 2007 for a comparison). If foliage grows or moves in relation to the position of the Sun (i.e., through phototropism and heliotropism), then its projection coefficient (projected area/leaf area) is a function of both the azimuth and zenith angles. If foliage is distributed symmetrically along all azimuths, however, then its

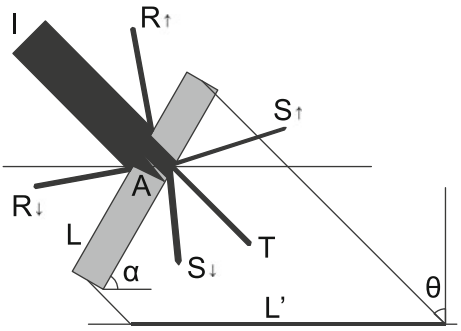


**Fig. 2.5** Schematic interaction of radiation with a leaf blade: $I$ = incoming radiation, $A$ = absorption, $R$ = reflection, $S$ = scattering, $T$ = transmission, $L$ = leaf area, $L'$ = projected leaf area on a horizontal surface, $\theta$ = zenith angle of the incoming radiation, $\alpha$ = leaf inclination angle. The *subscript arrows* denote the downward or upward components of the diffused radiation (each corresponding to one of the hemispheres delimited by a horizontal surface)

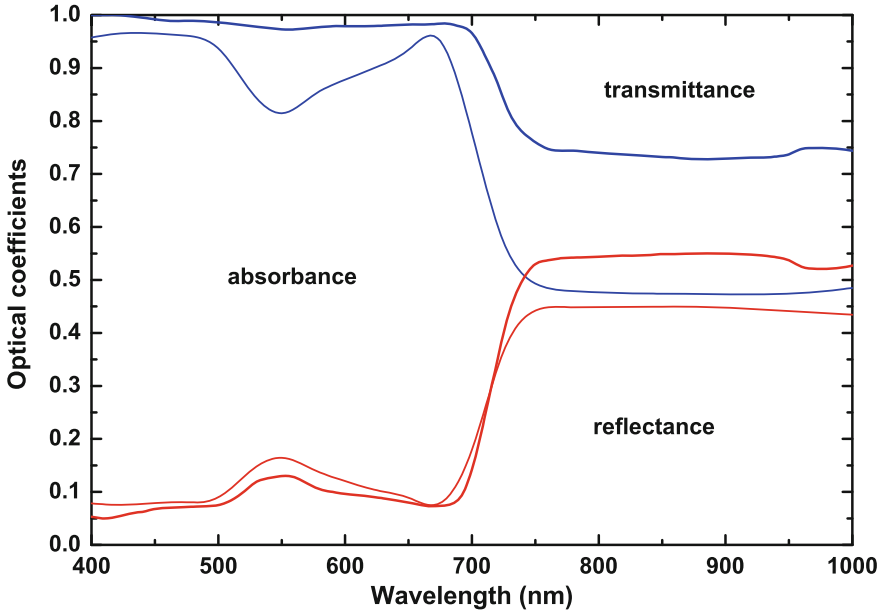


**Fig. 2.6** Typical spectra of leaves (*thin lines*) and needles (*thick lines*). Redrawn (simplified) from Berbigier and Bonnefond (1995) and Dai and Sun (2006)

projection coefficient is a function $G(\theta)$ of the zenith angle. The horizontal area $L'$ that is shaded by a leaf of area $L$ is then (Fig. 2.5)

$$L' = LG(\theta)/\cos\theta. \tag{2.21}$$

The leaf area index (LAI) is defined as the leaf area per unit ground area and, therefore, is a dimensionless quantity. Considering that leaves, and especially needles, are not perfectly flat, the leaf area itself is defined either as the maximum projected area or as half of the total three-dimensional surface. Direct radiation is reduced by the leaf area in a manner that can be expressed as a differential equation, such that

$$dI/dL = -(G(\theta)/\cos\theta)I = -kI, \tag{2.22}$$

where $k$ is the extinction coefficient of the canopy for direct radiation, which corresponds to an optical depth per unit leaf area. When integrated, this differential equation yields the Beer-Lambert-Bouguer law, such that

$$I(L) = I_0 e^{-kL}, \tag{2.23}$$

where $I_0$ is the radiation at the canopy top.

If $L$ is taken as the LAI above any level of the canopy, then this relation describes the attenuation of direct radiation as it enters the canopy. The fate of diffuse radiation is more complicated because it is not only absorbed by the leaves, but also is produced by scattering on them. Moreover, scattering occurs essentially in all directions; therefore, it must be described by an angular distribution that is a function of the incident and scattering angles, which is called a scattering phase function (Ross 1981). To simplify, scattering can be partitioned into an upward and a downward component, where both represent an angular integration over a hemisphere that is either below or above a horizontal surface (Fig. 2.5). If diffuse radiation is assumed to be isotropic, then a two-stream model can be used to model radiative transfer in a canopy (Dickinson 1983). The partitioning of scattering is first calculated via an "upscatter coefficient" $\beta$, which is the proportion of downward diffuse radiation that is scattered upward. Similarly, $\beta_o$ is defined as the upscatter of direct incident radiation. Consequently, the two coefficients are respectively calculated as

$$\beta = \left(\rho + \tau + (\rho - \tau)(\cos\alpha)^2\right)/2\omega \tag{2.24}$$

and

$$\beta_o = \frac{1 + \overline{\mu}k}{\omega\overline{\mu}k}\omega_s(\mu), \tag{2.25}$$

where $\rho$ is the leaf reflectance, $\tau$ is its transmittance, $\omega = \rho + \tau$ is its scattering coefficient, and $\alpha$ is the mean leaf inclination angle. The average inverse diffuse optical depth per unit leaf area $\overline{\mu}$ is

$$\overline{\mu} = \frac{1}{k'} = \int_0^1 \frac{\mu'}{G(\mu')} d\mu', \tag{2.26}$$

where $\mu'$ is the cosine of the zenith angle of the scattered radiation, and $k'$ is the diffusive extinction coefficient (all quantities in Eq. 2.26 are dimensionless). The single scattering albedo of the canopy $\omega_s$ is the proportion of scattering over the sum of scattering and absorption. It is a function of the scattering phase function and the angular distributions of both the radiation and leaves (Dickinson 1983; Sellers 1985). The downscatter coefficients are values that are complementary to the aforementioned upscattering coefficients (viz., $1 - \beta$ and $1 - \beta_o$, respectively). Without going into the details of the calculations, it is important to note that the reflectance (i.e., albedo) of a canopy is always smaller than that of a flat leaf; the former usually is not much more than half of the latter. This is due to radiation being trapped in the canopy, where each leaf is surrounded by other leaves. This offers new chances for the scattered radiation to be absorbed, especially in tall plant

canopies like forests (Stanhill 1970). Two separate equations that can be used then to describe upward and downward (isotropic) diffuse radiation are

$$\mu di_{\downarrow}/dL = \beta\omega i_{\uparrow} - (1-(1-\beta)\omega)i_{\downarrow} + \omega\mu k(1-\beta_o)\mathrm{e}^{-kL} \tag{2.27}$$

and

$$\mu di_{\uparrow}/dL = \beta\omega i_{\downarrow} - (1-(1-\beta)\omega)i_{\uparrow} + \omega\mu k\beta_o\mathrm{e}^{-kL}, \tag{2.28}$$

where $i = I/I_0$. In other words, both components (up and down) of diffuse radiation are the result of their own and respective scattering. together with the scattering of direct radiation.

When these differential equations (Dickinson 1983) are integrated (Sellers 1985) by choosing appropriate angular distributions for the foliage and by setting the radiation that is reflected by the soil beneath the canopy, they yield

$$I_{\uparrow} = \rho_{soil}\left(I_{\downarrow} + \mathrm{e}^{-kL}\right). \tag{2.29}$$

It is also possible to use a discrete ordination method that consists of defining a finite number of cells in the canopy space and a finite number of directions in space (Myneni 1991). Obviously, this method is computationally intensive. In Eqs. 2.27 and 2.28, the same value of $\beta$ is used for the upscatter of downward diffuse radiation as for the downscatter of upward radiation. However, the optical properties of both leaf sides can differ. Dai and Sun (2006) introduced this difference in a generalized model, together with anisotropic incoming radiation. Their model is too complicated to be described here in detail. Its main result is a difference in overall reflectance of the canopy compared to the two-stream model. Depending on the leaf angle, on the proportion of direct or diffuse incoming radiation, and on the wavelength, this difference (positive or negative) can be significant (Dai and Sun 2007).

Compared to a canopy in which all leaves would be black, scattering increases transmittance and reduces the absorbance of a canopy. As suggested by Fig. 2.6, reflectance and transmittance of annual leaves are often similar, while persistent leaves and conifer needles exhibit low transmittance. For leaves with $\rho = \tau$, it can be shown that scattering decreases the effective extinction coefficient of a canopy by a factor $\sqrt{\alpha}$. This rule applies to flat leaves and approximately to non-flat ones. The extinction of diffuse radiation through the canopy can thus be described with a single differential equation of the same form as Eq. 2.23, but with an adapted value for $k$ (Goudriaan 1977). A further method consists of using probabilities in describing the interactions of each photon with any leaf and calculating the resulting probabilities through the canopy with a Markov chain. This approach was used, for example, to assess the effect of within-shoot scattering, which accounts for the fact that leaves are not distributed randomly in the whole volume of a canopy but are grouped around shoots (Smolander and Stenberg 2005).

Models of radiation transfer in canopies are often used in remote sensing. In the visible range, the soil and vegetation are both dark. In the near-infrared band,

however, vegetation has a lower absorbance than soil. Measuring the reflectance in both bands thus allows the LAI and the fraction of absorbed PAR (FAPAR) of vegetation canopies to be estimated (Tucker 1979; Sellers 1985). In fact, a forest canopy, as seen from above, includes not only its trees but also its shrub, herb, and moss layers. This is especially important when comparing ground-based measurements with aerial or satellite data.

In the analysis of hemispherical photographs, vegetation is often separated from the visible sky by segmentation of the original colors or gray values into black and white. This corresponds to setting the absorbance of canopy elements to $\alpha = 1$ and allows the simpler Eq. 2.23 to be used. It should be noted that $I$ in this equation is an average, but direct radiation actually produces sunflecks and shadows rather than uniform average radiation (Way and Pearcy 2012). The same remark applies when slopes that are more or less exposed to the Sun are compared. In this case, different radiation fluxes are calculated using Iqbal's equation (Eq. 2.17) and, within the canopy, Eq. 2.22 must be replaced with that of Schleppi et al. (2007), i.e.,

$$I(\theta, \gamma) = I_0(\theta, \gamma) \mathrm{e}^{-G(\theta) L \cos \nu / \cos \gamma}, \tag{2.30}$$

where $\nu$ is the slope angle and $\gamma$ is the angle of incidence (see Eq. 2.12 for its calculation). Note that we use here L per projected area while it is considered per inclined area in Schleppi et al. (2007). Varying slopes and aspects will result in different average irradiances within the canopy, but this corresponds to different proportions of sunlit versus shaded leaves and not to a proportional modification of direct radiation (Wang et al. 2002). As depth into the canopy increases, sunflecks and shades are no longer sharp because the sunrays are not exactly parallel. With an apparent sun diameter of 0.009 rad, there is a fringe of penumbra measuring 9 mm at a distance of 1 m from the object casting shade. Because they increase proportionally with distance, these penumbral effects are especially important for herb layers beneath large trees (Smith et al. 1989).

### 2.5.2 *Photosynthesis Models*

Different models of radiation penetration form the basis of photosynthesis models. Theoretical developments in these respective fields are thus linked. In the simplest case, the entire canopy is lumped together and considered as one entity. This is known as the "big-leaf" model, where incident PAR is equally partitioned over the whole leaf area and photosynthesis is driven according to a saturating response curve. This model does not directly take into account that individual leaves receive different irradiances and that they are adapted to different irradiance regimes over time. Under certain assumptions, both of these sources of variation may indeed cancel one another out and result in a correct model (Sellers et al. 1992). In most cases, however, these effects have to be taken into account indirectly through empirical parameters and response curves. Further, it has been shown (de Pury and

Farquhar 1997) that these corrections are themselves affected by the leaf area index and by the nitrogen content of leaves.

A more mechanistic approach considers sunlit and shaded foliage separately (e.g., Sinclair et al. 1976). This "two-big-leaf" model is quite effective because photosynthesis in sunflecks is light-saturated most of the time, while in the shade it varies with PAR in an approximately linear fashion. Both processes are well described by simple equations. Further, overestimation that is due to the averaging of radiation along the photosynthesis response curve (Smolander 1984) is avoided. Such models are considered to be a good compromise between simplicity and accuracy (de Pury and Farquhar 1997). Yet another way to avoid overestimation of photosynthesis is to use light data with a high temporal resolution in conjunction with a light-response curve (Paquette et al. 2010).

In more sophisticated models, the canopy is divided into several layers (e.g., Norman 1982; Aber and Federer 1992; Berbigier and Bonnefond 1995). In each layer, radiation is partitioned into absorption and scattering (up and down). Direct and diffuse radiation can be treated separately, as has been previously explained. An important advantage of these models is that changes in leaf morphology and physiology can be integrated with canopy depth. Indeed, leaves that are adapted to shade have lower photosynthetic capacity, lower specific mass and lower nitrogen concentrations compared to leaves at the top of the canopy (Posada et al. 2009). These trends are very generally observed even if species and stress factors also affect photosynthesis. Sellers et al. (1992) explained this robustness as an optimization of resource allocation both within the plant and within the canopy. Nitrogen plays a prominent role for plants because it represents, along with carbon, a heavy investment in the photosynthetic machinery (particularly, the Rubisco enzyme). In these models, radiation, water, carbon and nitrogen intimately interact throughout the canopy.

### *2.5.3 Canopy Structures*

In the preceding sections, we implicitly treated canopies as leaves that were distributed randomly in horizontal directions and, therefore, as horizontally homogenous (at scales larger than the size of leaves). Scattered radiation is not very sensitive to this randomness assumption (Ross 1981), but direct radiation is. In reality, plants feature different aboveground organs (stems, branches, leaves, flowers, fruits) and the overall architecture of the stand depends on their morphology (Ross 1981). In forests, two levels of canopy structure can be distinguished: first, the distribution of single trees in the stand, and second, the architecture of single trees (Côté et al. 2015). The distribution of trees over an area is the main feature of so-called "gap-models," which are individual-based, spatially explicit forest models that mainly describe population dynamics (e.g., SORTIE-ND; Canham and Murphy 2005). These models describe reproduction, growth (including rough morphological parameters), and mortality of trees. All

three processes can be directly affected by light, which can thus regulate competition between individuals and between species. Species can be affected by light as early as during germination. While some species need light to germinate, others require darkness, whereas many are light-insensitive. Borthwick et al. (1952) discovered that this response is due to red light (650–680 nm), but germination can be repressed by subsequent exposure to far-red light (710–740 nm; i.e., wavelengths at the border between visible and near-infrared). The pigment phytochrome is responsible for these responses in plant cells (Butler et al. 1959). Phytochrome controls germination as well as different morphological effects of light (i.e., photomorphogenesis), including the influence of day-length on flowering (i.e., photoperiodism). It must be noted that these mechanisms are independent of photosynthesis and take place even at low radiation levels. The spectral band controlling the phytochrome system is narrow, but it corresponds to a sharp change in leaf optical properties (Fig. 2.6); therefore, the red/far-red ratio (R/FR) is strongly reduced in a plant canopy (e.g., Brasseur and de Sloover 1976). The red/far-red ratio is used by plants, along with sensitivity to blue light, to sense the presence of possible competing plants even before they can have an effect on photosynthesis through mutual shading (Ballaré 1999).

The shape of single trees is affected by light: this is easily observed by comparing trees that have been growing together in a forest versus solitary individuals, or by comparing stands on slopes with different aspects (Ameztegui et al. 2012). Three mechanisms are responsible for these differences: photomorphogenesis, growth as affected by photosynthesis, and mortality of branches due to a lack of light. The effect of light on tree seedlings, for example, was studied in situ by Roussel (1972), who showed etiolation at low light levels (i.e., growth that is characterized by longer but weaker shoots, and smaller roots), and by Paquette et al. (2007a), who showed that species adaptations to shade were expressed through phenotypic plasticity. Etiolation is a photomorphogenetic effect that can be understood as a strategy for increasing the chances that a seedling reaches a height with more available light (e.g., above litter or mosses). From their second or third year onwards, most coniferous tree seedlings become insensitive to this morphogenetic effect. Their growth form is then largely determined by apical dominance. As a consequence, the effects of radiation become limited to growth rates (via photosynthesis) and to the shedding of lower branches receiving insufficient light. However, some differences exist within conifers: *Pinus* branches, for example, retain the ability to grow asymmetrically in response to light, while species such as *Pinus mugo* or *Taxus canadensis* adopt a shrub-like growth form with multiple stems. As already noted by Engler (1924), broadleaved trees remain affected by photomorphogenesis throughout their lives; therefore, as large trees, they are better able to take advantage of small canopy gaps by growing into them. As a result, at similar stem densities, broadleaved or mixed canopies generally exhibit fewer gaps and capture more incoming light than do coniferous ones (e.g., Gower and Norman 1991; Frazer et al. 2017).

Some models have been developed to simulate the morphology of branches of whole trees based on relatively simple growth rules. Tree morphology can then be

used to populate small-volume cells (viz., voxels) with leaves. Myneni (1991), for example, tested his discrete ordination method (see Sect. 2.5.1) on *Populus* trees by simulating their crown structure with fractal geometry. Similarly, Langensiepen et al. (2006) modeled the radiation regimes, photosynthesis and transpiration of *Eucalyptus* trees. Working with very open canopies, they were able to derive the three-dimensional morphology of trees from photographs that were taken from below and from the side. It is also possible to derive allometric equations from detailed destructive measurements (e.g., Porté et al. 2000), but the method is time-consuming, and the acquisition or verification of three-dimensional data remains a challenge. Ground-based LIDAR is also in the process of being developed as a tool for assessing the three-dimensional structure of trees (Côté et al. 2009).

The problems of explicit tree crown models are avoided by the gap-size approach of Chen and Cihlar (1995). Gaps in the canopy can be measured as sunflecks on the ground. Gaps within tree crowns are small; their size is of the same order of magnitude as leaves. Gaps between trees, in contrast, are much larger. From the probability distribution of their sizes, between-crown gaps can thus be separated from within-crown gaps. The whole canopy is then regarded as a juxtaposition of leaf-populated areas (i.e., the crowns) and empty spaces. In the original method using sunflecks to estimate leaf sizes and canopy clumping, measurements are taken only in the direction of the Sun. Using HP, however, it is possible to extend this approach to all zenith angles; this can be done by using several software packages (Frazer et al. 2017; Hall et al. 2017). The structure of the forest stand (i.e., tree pattern type and size) can even be inferred from the variance of gaps detected in hemispherical photographs (Montes et al. 2008).

### 2.5.4 Energy Budgets

In addition to photosynthesis, growth, and morphogenetic effects, solar radiation has a crucial effect on forests by determining their energy budgets and, consequently, their temperatures. As shown above, leaves absorb mainly the visible portion of incoming solar radiation, and they largely scatter its near-infrared component. The thermal radiation that is emitted by plants and soils is in the longwave (thermal) infrared range. According to the Stefan-Boltzmann law, emitted power is proportional to the fourth power of the absolute temperature $T$. The emitted radiative flux $j$ is defined as

$$j = \varepsilon \sigma T^4, \tag{2.31}$$

where ε is the emissivity of the surface relative to an ideal black body, and σ is the Stefan-Boltzmann constant. Foliage has a high emissivity (typically between 0.94 and 0.99); it also has a high absorbance at these wavelengths (typically near 0.95) and practically no transmittance. The absorbed energy that heats the leaf tissues can

be reemitted in all directions as though it were being scattered. As a result, a plant canopy acts as greenhouse for thermal radiation because it partly reemits the thermal radiation that is coming from the soil.

The radiation budget at Earth's surface is the sum of shortwave and longwave budgets (Geiger et al. 2009). The net radiation budget $Q^*$ is

$$Q^* = K + L = K_{\downarrow} - K_{\uparrow} + L_{\downarrow} - L_{\uparrow}, \tag{2.32}$$

where $K_{\downarrow}$ is the solar shortwave radiation, $K_{\uparrow}$ is the reflected shortwave radiation, $L_{\downarrow}$ is the longwave radiation from the atmosphere, and $L_{\uparrow}$ is the emitted longwave radiation. The total energy budget at the canopy top also includes the exchange of heat. The energy accumulating in the ecosystem $Q_S$ is represented as

$$Q_S = Q^* + Q_H + Q_E + Q_R, \tag{2.33}$$

where $Q^*$ is the net radiation budget, $Q_H$ is the heat transported by air convection and advection, $Q_E$ is the latent heat of water vapor, and $Q_R$ is the heat brought by precipitation. Most of these energy fluxes are bidirectional, and their sign has to be defined by convention. In Eq. 2.33, fluxes into the system are considered positive and fluxes flowing out of the system are negative. For example, evapotranspiration represents a negative $Q_E$. Within the ecosystem, there are further exchanges between above- and belowground components, which can be summarized as

$$Q_S = Q_G + Q_B + Q_A + Q_V + Q_P, \tag{2.34}$$

where $Q_G$, $Q_B$, and $Q_A$ are the net heat storage into the soil, the above-ground biomass, and the air, respectively. The term $Q_V$ is the latent heat of water vapor within the canopy and $Q_P$ is the energy used by net photosynthesis (i.e., gross photosynthesis minus ecosystem respiration). The net energy that is absorbed by photosynthesis and accumulated as chemical biomass energy is usually very small compared to radiative and thermal fluxes. It is not generally possible or necessary to measure all components of the energy balance. Rather, for most applications, it is sufficient to directly measure or model major components and to use coarser approximations or assumptions for minor fluxes. HP can provide important parameters (e.g., gap fraction, LAI, mean leaf angle) for such applications (Leblanc and Fournier 2014, 2017).

The energy budget of a forest is important in that it determines the temperature regime of the trees, other plants and the soil. The energy budget affects all physiological processes including photosynthesis, transpiration, translocation, and growth. The temperature regime is important for all microbiological soil processes, for root growth, and for the uptake of water and nutrients. Over an entire day, $Q_S$ is approximately zero (Eq. 2.33). During the day, $Q^*$ is positive while $Q_S$, $Q_H$, and $Q_E$ are negative: radiation is a source of energy, which goes mainly into the ecosystem (viz., the soil) or is released as latent heat into the atmosphere. At night, $Q^*$

becomes negative, as do $Q_S$ and $Q_G$: heat that is stored in the soil is lost by longwave radiation. During the day, the air temperature is generally lower under a forest canopy than in open sites. This effect is especially marked in the morning and during hot, sunny days (Renaud and Rebetez 2009). Because of its height, a forest canopy absorbs incoming radiation in a large volume where convection and evapotranspiration can effectively remove part of this energy (i.e., negative $Q_H + Q_E$). In the canopy of low-statured plants, in contrast, radiation energy is kept within a small volume, which is aerodynamically less tightly coupled to the free atmosphere. The consequence is a higher temperature in both the vegetation and soil. This difference between trees and herbaceous plants was shown to be the main cause of altitudinal tree lines (Körner 2007). At night, when there is no incident shortwave radiation, the temperature is usually higher under a canopy Canopydue to the reflection of emitted thermal radiation (i.e., lower $L_{\uparrow}$). For example, the presence of trees can effectively prevent grass from freezing in a silvopastoral system (Feldhake 2002). The combination of day and night effects results in lower soil temperatures under trees compared to open land (e.g., Hawke and Wedderburn 1994).

An important application of energy budgets is for understanding and predicting snowmelt. Snow interception, sublimation, and melt are all affected by the presence of trees. For example, LaMalfa and Ryle (2008) observed that more snow accumulates in meadows than in coniferous forests, with deciduous forests taking an intermediate position. Burch et al. (1996) found comparable differences and could explain the reduced snow accumulation in forests only by a combination of interception and sublimation from tree crowns over the winter. The necessary energy is provided by solar radiation, which is much better absorbed by a forest canopy (even without leaves and partly under snow) than by continuous snow cover where the albedo is very high. Within a forest stand, variability in the canopy cover and topography affect the patterns of both snow accumulation and melt (Essery 1998; Stähli et al. 2009).

## 2.6 Radiation Sensors and Their Use in Forests

Radiation above, within, and under forest canopies is variable in time, space, direction, and wavelength spectrum. There is no measuring device that takes all of these seven dimensions into account at once: one dimension for time, three for space, two for direction, and one for wavelength. Different instruments are available for different applications. In this section, we give a very short overview of their possibilities and limitations. While a more detailed review can be found in Pearcy (1989), here we include a description of new sensor technologies that have recently become available. Table 2.1 summarizes the main strengths and limitations of different instruments.

**Table 2.1** Strengths and limitations of different instruments and techniques that are used to assess radiation, especially in forests

| Instrument | Precision and accuracy | Time dimension | Space dimensions | Directions (azimuth and elevation) | Defined wave-length band(s) |
|---|---|---|---|---|---|
| Actinometers | ++ | + | ± | – | + |
| Spectroradiometers | + | + | ± | – | ++ |
| PAR sensors | + | + | ± | – | + |
| Ceptometers[a] | + | ± | + | – | + |
| Mobile systems[b] | + | ± | ++ | – | ± |
| Plant canopy analyzer[c] | + | – | ± | ± | ± |
| Multi-angular systems[d] | ± | ± | ± | + | ± |
| Photography | – | – | ± | ++ | – |

We compare how well the different dimensions of a radiation measurement are covered, with respect to time and location of the measurement, direction of the radiation, and its wavelength bands. See Sect. 2.8 for more details

[a]E.g., AccuPAR (Decagon, Pullman, WA, USA)

[b]Based on actinometers or PAR sensors, e.g., TRAC (Decagon), DEMON (CSIRO, Canberra, ACT, Australia)

[c]E.g., LAI-2000 (LI-COR Biosciences, Lincoln, NE, USA)

[d]E.g., BF5 (Delta-T Devices, Burwell, Cambridge, UK)

### *2.6.1 Actinometers*

Actinometers are broadband radiation energy sensors. Shortwave and longwave radiation can be precisely measured by heating a black thermopile (i.e., a sensor that converts heat into electrical energy). The radiation emitted by the sensor itself can be corrected using the Stefan-Boltzmann equation (Eq. 2.31). An actinometer following the track of the Sun that measures only direct radiation is called a pyrheliometer; a sensor that is used to measure global radiation from the sky is called a pyranometer; a pyrgeometer is an actinometer that is designed to measure longwave radiation from the Earth's surface. Net radiometers are composed of either two or four sensors, one up and one down (or two of each), for shortwave and longwave radiation, respectively (Fig. 2.7). Shortwave sensors have a glass dome that is transparent to visible and near-infrared radiation, while longwave sensors are equipped with a silicon surface that is transparent only to longwave radiation. The star pyranometer has a special design, where the difference between its black and white sectors is measured; as a consequence, the instrument is less sensitive to temperature changes (Table 2.2).

Thermopile actinometers are relatively expensive but precise instruments. Their calibration is subject to international standardization (ISO 9060), with the reference being held by the World Radiation Centre in Davos, Switzerland. Actinometers are

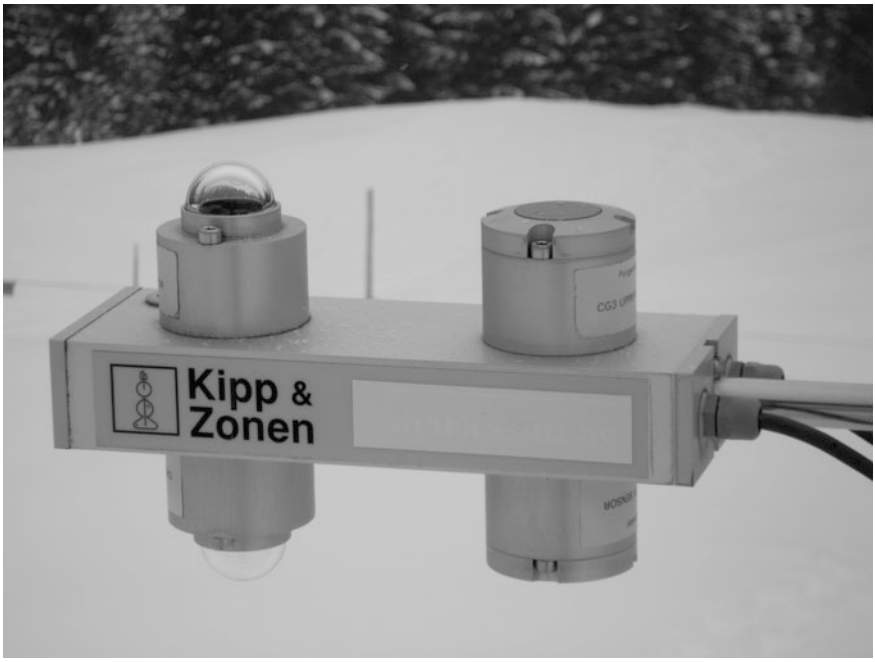


**Fig. 2.7** Net radiometer measuring shortwave and longwave radiation, downward and upward. Note the glass dome of the pyranometers and the flat silicon window of the pyrgeometers. *Photograph* Patrick Schleppi

typically used in standard weather stations (i.e., open-field stations). For shortwave radiation, photodiodes can be used instead of thermopiles. Photodiodes are electronic components that directly convert light into an electrical current. They are less expensive than thermopiles, but are also less precise.

### *2.6.2 Spectroradiometers*

Studying a radiation spectrum requires an instrument that is able to scan the spectrum in typically one or several steps per nm, as shown in Fig. 2.1. Spectroradiometers that are used in ecological studies measure wavelengths ranging from 300–350 nm to 1000–1100 nm (i.e., from the near-ultraviolet into the near-infrared). In some models, the receptor is linked to the measurement unit by fiber optics. Spectra that are produced by such instruments are useful in describing radiation as it affects plants (e.g., photosynthesis, photomorphogenesis) and animals (e.g., vision). In forests, spectra can differ appreciably according to the form of the incoming radiation (direct or diffuse) and to the presence and size of gaps (Endler 1993).

**Table 2.2** Comparison of light availability indices derived from HP analysis (e.g., GLI) and other methods for estimating understory light availability in different forest types

| Source | Forest type | Benchmark | Method | r[a] | HP performance |
|---|---|---|---|---|---|
| Paquette et al. (2007b) | Temperate deciduous (mature to pioneer) | Overcast $T_{PAR}$[b] | HP | 0.93 | Among best—less accurate in deep shade |
| | | | BF2[c] | 0.94 | |
| | | | Densiometer[d] | 0.91 | |
| Gendron et al. (1998) | Young deciduous coastal forest | Growing season $T_{PAR}$[e] | HP | 0.97 | Among best |
| | | | DIFN[f] | 0.95 | |
| | | | Overcast $T_{PAR}$ | ~0.95 | |
| | | | Instantaneous sunny day $T_{PAR}$ | 0.82 | |
| | | | Average sunny day $T_{PAR}$ | 0.92 | |
| Comeau et al. (1998) | Mixedwood (with a deciduous overstory) | Growing season $T_{PAR}$ | HP | 0.98 | Among best |
| | | | Average sunny day $T_{PAR}$ | ~0.96 | |
| | | | Overcast $T_{PAR}$ | 0.99 | |
| | | | DIFN | 0.99 | |
| | | | Densiometer | 0.96 | |
| Rich et al. (1993) | Tropical rainforest | Growing season $T_{PAR}$ | HP | ~0.87 | Not available |
| Easter and Spies (1994) | Mature and old-growth conifer coastal forests | Growing season $T_{PAR}$ | HP | ~0.96 | Not available |
| Battaglia et al. (2003) | Longleaf pine forest | Growing season $T_{PAR}$ | HP | 0.88 | Best |
| | | | Average sunny day $T_{PAR}$ | ~0.39 | |
| | | | Overcast $T_{PAR}$ | ~0.76 | |
| Machado and Reich (1999) | Conifer-dominated temperate forest | Mean daily $T_{PAR}$ | HP | 0.74 | Good overall—less accurate in deep shade |
| | | | Overcast $T_{PAR}$ | 0.96 | |
| | | | DIFN | 0.96 | |

When available, the authors' evaluations of the relative performance of HP are also given

[a]When $r^2$ coefficients were published, they were converted to correlations ($r$) for uniformity's sake. ~ denotes an estimated average from several similar results

[b]PAR transmittance estimated instantaneously using quantum sensors under an overcast sky (Messier and Puttonen 1995; Parent and Messier 1996)

[c]Developed as an alternative to the overcast method using a hemispherical PAR sensor array (BF2, Delta-T Devices, Burwell, Cambridge, UK). Now replaced by model BF5

[d]Results from a spherical densiometer (Forest Densiometers, Arlington, VA, USA) were published only online: https://www.researchgate.net/publication/248428385_A_less_restrictive_technique_for_the_estimation_of_understory_light_under_variable_weather_conditions

[e]Growing season PAR transmittance standard (see text)

[f]Diffuse non-interceptance of blue light as measured with a plant canopy analyzer (LAI-2000, LI-COR Biosciences, Lincoln, NE, USA)

### 2.6.3 PAR Sensors

Photosynthetically active radiation (PAR, defined as the radiation between 400 and 700 nm; see Sect. 2.4) is commonly measured with sensors that are based on photodiodes and equipped with filters to restrict their response range. Instruments from different manufacturers may differ in their actual response curves to these wavelengths (for an example, see Fig. 2.8). Over its spectrum, photosynthesis is more closely related to the number than to the total energy of photons in the radiation flux (McCree 1972). For this reason, PAR is commonly measured as a photosynthetic photon flux density (PPFD), which is expressed in moles of photons (or Einsteins); the corresponding instruments are called quantum sensors.

### 2.6.4 Distributed Systems

Because of their relative affordability, multiple photodiodes (i.e., PAR sensors or others) can be used in an array within or under a plant canopy, thereby capturing the spatial and temporal heterogeneity of radiation. To measure sunflecks in small canopies, it is possible to group sensors along a bar to create what is referred to as a

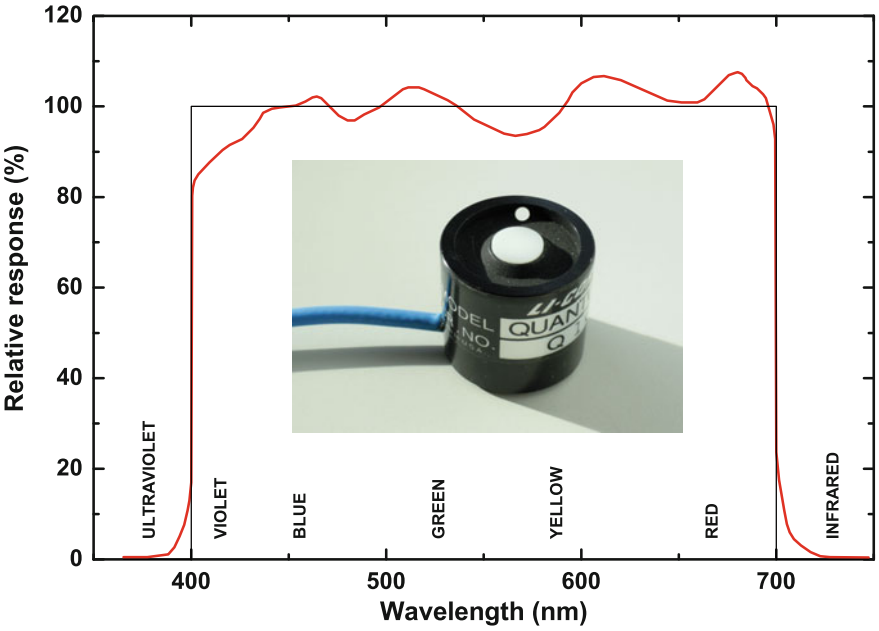


**Fig. 2.8** A quantum sensor and its response curve with respect to the ideal response (equal for all photons in the 400–700 nm waveband—*thin black line*). Graph redrawn from LI-COR Biosciences (Lincoln, NE, USA); *photograph* Patrick Schleppi

"ceptometer" (e.g., AccuPAR, Decagon, Pullman, WA, USA). In forest canopies, it is often necessary to perform measurements at distances that are greater than the length of a ceptometer. Thus, mobile devices have been developed to simultaneously measure both the radiation and position of the sensor. While some systems are commercially available (e.g., TRAC, Decagon, Pullman, WA, USA; DEMON, CSIRO, Canberra, ACT, Australia), it is also possible to fit one or more sensors onto a small wagon that travels along a rail (e.g., Stähli et al. 2009). Each measurement point is then visited at defined time intervals and a single sensor is able to capture variability in both time and space.

### 2.6.5 *Angular Systems Including Photographic Sensors*

Different systems exist that simultaneously measure radiation coming from different directions. These so-called plant canopy analyzers (e.g., LAI-2200, LI-COR, Lincoln, NE, USA) measure blue light within a series of concentric rings and are specially designed to measure LAI of the canopy.

Photodiodes mounted on platforms that rotate horizontally and vertically can scan the entire sky vault and are called sky scanners. Typically, they take measurements at more than 100 discrete angular positions and are mainly used to measure sky luminance (see Sect. 2.3). A static counterpart of the sky scanner is the so-called Solar-Igel, which has 135 sensors covering the sky hemisphere (Appelbaum 1987).

One of the major challenges in measuring the light that is available below forest canopies is accounting for direct light (i.e., sunflecks through gaps) in one or several instantaneous measurements. Two handheld devices enable the observer to view an image of the canopy above them: the spherical densiometer (Lemmon 1956) and the horizontoscope (Schütz and Brang 1995). Their main advantage lies in in situ assessment of canopy coverage, which makes them useful as decision-making tools for practical purposes such as tree planting or felling. Fisheye photographs provide essentially the same information but record it; this allows more precise analysis as will be shown in the remainder of this chapter and in Leblanc and Fournier (2014). Several other methods have also been developed using light sensors (see Gendron et al. 1998). One of the most recent attempts relies on a new sensor array that uses seven photodiodes located under a hemispheric dome with a shading pattern arranged in such a way that at least one sensor is always measuring both direct and diffuse light. The BF5 and SPN1 sunshine sensors (Delta-T Devices, Burwell, Cambridge, UK) require no adjustment of a shade-ring to track the Sun; thus, they can be used at any latitude and under any sky condition (e.g., overcast to sunny). To evaluate available light, two simultaneous measurements are taken (a) under the canopy to be evaluated, and (b) in a nearby open field. Using only the diffuse signal from both sensors, available light is simply the *a*/*b* ratio, thereby integrating direct light from all gaps throughout the daily and seasonal course of the Sun in one single measurement (Paquette et al. 2007b).

All photographic instruments can also be considered as angular measuring devices since they record radiation in an array of angles and then project these

measurements onto an even surface. The quantitative analysis of photographs is done by computer software that uses digital or scanned images as input. Sensors in digital cameras are arrays of photodetectors. Two main types exist: charge-coupled devices (CCD) and active-pixel sensors (APS). While the first requires separate amplification of the signals that are obtained, the second integrates acquisition and amplification within a single integrated circuit. Most color cameras use an interlaced grid of sensors for red, green, and blue colors (RGB) in a ratio of 1:2:1. Special designs use three layered grids or three separate arrays. To produce conventional file formats, the raw readings are converted to bring all three color values into single pixels. While consumer-grade cameras are equipped with RGB sensors, more specific detectors are used in astronomy and remote sensing; for example, they can measure different bands of radiation.

The first purpose of consumer-grade photography is to record subjective color patterns to form images and not to produce absolute radiance readings. As a consequence, the RGB values of the files that are produced should not be considered as an accurate measure of radiation. There is especially loss of brightness (or saturation) from the center towards the edges of the photograph. This effect, which is called "vignetting," is due to the geometry of the lens and sensor. It increases with the aperture of the lens. There is also a limitation in the dynamic range because RGB values are limited in common formats to values between 0 and 255 (8 bits per color). Photographs are encoded on a scale that is adapted to the sensitivity of human vision through a power function, where the exponent is denoted $\gamma$ (hence "gamma encoding"), such that

$$Y = X^{\gamma}, \tag{2.35}$$

where $Y$ is the encoded brightness and $X$ is the physical radiance (in arbitrary units). Typical values that are used for $\gamma$ are 1.8 or 2.2.

When light saturation occurs on the sensor, light patches can appear larger than they really are. This "blooming" effect (Leblanc et al. 2005; Thimonier et al. 2010) is due to the electronic excitation of sensor pixels that spills over onto neighboring pixels.

In addition to conventional photography in the visible range, near-infrared (NIR) photography can also be used in forests. Combining both techniques into a single instrument permits what is referred to as "multiband vegetation imaging" (MVI, Kucharik et al. 1997). The main advantage of this technique is that it can differentiate between branches, shaded leaves, and sunlit leaves under different sky conditions.

## 2.7 Hemispherical Photography

### *2.7.1 Principles and Development*

HP uses a lens, which is called a "fisheye," with a very short focal distance. Thus, the field of view (FOV) is very broad, essentially 180° ($\pi$ rad). The hemisphere that

is seen by the lens is projected as a disk onto the film or sensor of the camera. When the camera is directed upward, the circle on the image corresponds to the horizon. Each point within this circle is then defined by its polar coordinates. The angle on the image corresponds to the azimuth in reality, while the relative radius corresponds to the zenith angle via

$$\theta = f(r/R)\pi/2, \tag{2.36}$$

where $r$ is the distance to the center and $R$ is the radius of the image (i.e., the distance between the projected zenith and horizon). The function $f$ is a monotonically increasing function describing the geometry of the image that is produced by the fisheye lens, where $f(0) = 0$ and $f(1) = 1$. Each lens type has its own geometry, which is usually determined by fitting a polynomial regression to measurements taken in a known setup of the camera and targets.

Interestingly, the SORTIE individual-based forest simulator (Canham and Murphy 2005) models the canopy as a hemispherical photograph. Indeed, for every simulation run, fisheye pictures are generated over every tree for which the model needs to compute light availability, and it analyzes them in the same manner as the actual fisheye photographs that are used to compute light availability indices (e.g., the Gap Light Index, see Sect. 2.7.2 below and in Jonckeere et al. (2017). The SORTIE model has been or is being parameterized for many forest ecosystems around the world using real hemispherical photographs to determine species-specific crown openness and to validate the model by comparing simulated and observed light (e.g., Pacala et al. 1996; Canham et al. 1999; Beaudet et al. 2002).

Historically, upward HP was first used by Hill (1924) to take pictures of the sky with clouds. Evans and Coombe (1959) drew sun tracks on pictures taken in forests to study the direct radiation below the canopy. Anderson (1964) provided the theoretical basis for using hemispherical photographs to estimate diffuse radiation. Bonhomme and Chartier (1972) introduced the automatic digitization of photographs, which enabled the first wave of research in forests. The theory was refined in the late 1980s (Pearcy 1989; Rich 1990). A second wave of research and applications arose when digital photography became broadly available around the year 2000.

Compared to other techniques, HP has the advantage of providing a permanent record of canopy geometry. This record is essentially valid as long as the geometry does not change (e.g., foliage growth or shedding, tree growth or removal). The directional geometry of transmission through canopy openings is identified as visible sky directions, while interception by canopy elements is identified as obscured sky directions. The objective of image analysis is therefore not to measure the prevailing light conditions directly but to infer them from the obtained photograph (Rich 1990). HP can easily be repeated over time to cover seasonal or interannual variation. It can also be repeated at different locations, thereby taking spatial variability into account. Two main fields of application can be distinguished (Fig. 2.9): local analysis (e.g., Zlatanov et al. 2013) versus canopy analysis (e.g., Thimonier et al. 2010).

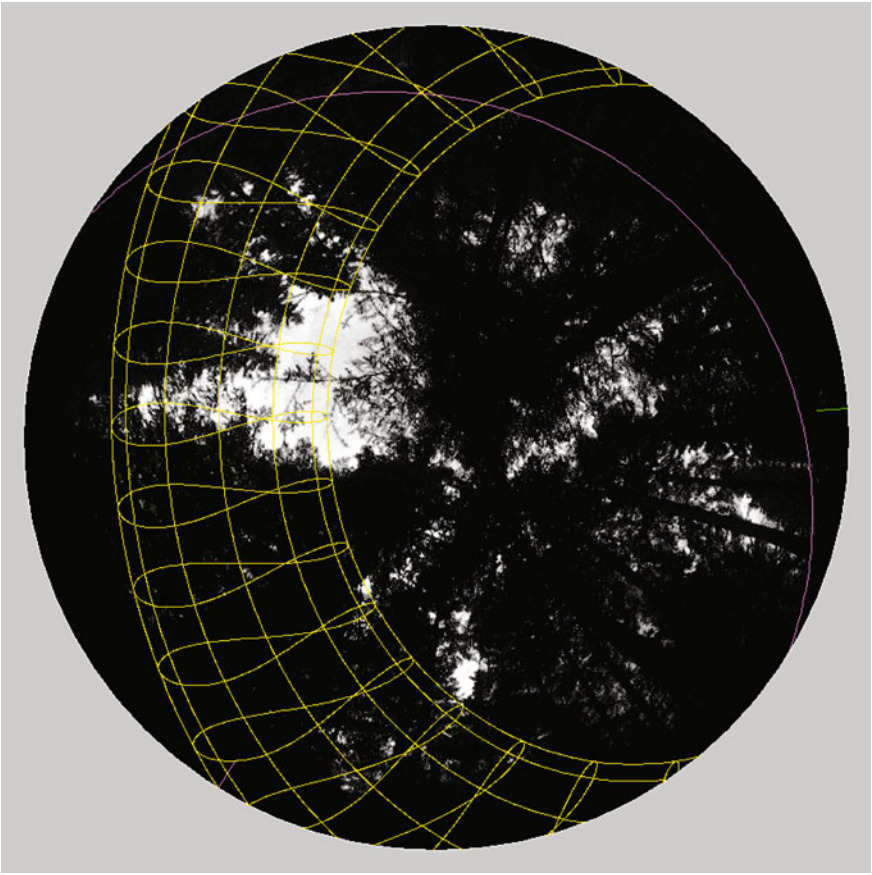

**Fig. 2.9** Hemispherical photograph of a *Picea abies* forest in Alptal, Switzerland. The *parallel lines* indicate the path of the Sun every month and the *eight-shaped lines* show its position at full hours. The *top right curve* indicates the position of the ground (slope of 11°). Over the year, assuming that ¼ of the solar radiation directly reaches the canopy, it delivers 10 W $m^{-2}$ at the position of the photograph. Solving the model of Campbell (1986) using a weighted least-squares approach (Schleppi et al. 2007) gives an effective LAI of 3.30 and a clumping-corrected LAI (Chen and Cihlar 1995) of 3.67, with an average foliage angle of 61°. These values correspond to a direct solar radiation value of 5 W $m^{-2}$ on average under this canopy. The fact that local direct radiation is twice as high as the average is due to the large gap to the south. For diffuse radiation, depending upon the selected model, the local value and the canopy average are both around 5 W $m^{-2}$. *Photograph* Patrick Schleppi

### 2.7.2 Local Analysis

Local analysis, or point analysis, of hemispherical photographs aims to describe the radiation regime at the point at which each image is taken. The visible part (viz., the black-and-white "viewshed") of the canopy is first extracted from the image to

determine for each pixel whether radiation is transmitted or blocked. This viewshed is then combined with a model of above-canopy incoming radiation to calculate the transmitted radiation for a given period (e.g., a growing season). This calculation is done over time based on the position of the Sun, its direct radiation, and patterns of diffuse radiation (see Sects. 2.2 and 2.3). A relatively simple index is often used for the evaluation of the understory light climate and is referred to as the gap light index (GLI, Eq. 2.37), which is also called the global site factor (GSF) (Canham 1988; Rich et al. 1993). The gap light index $T$ is given by

$$T = p_{dir} T_{dir} + p_{dif} T_{dif} \tag{2.37}$$

where $p_{dir}$ and $p_{dif}$ represent the proportions of incident light (above canopy) that are respectively direct and diffuse, and $T_{dir}$ and $T_{dif}$ are the proportions of each fraction reaching the understory (i.e., transmitted through gaps). The term $T_{dif}$ is often called diffusive non-interceptance (abbreviated DIFN or DNI). The $p$ factors can be either measured or modeled, and the corresponding transmittances $T$ are derived from photographs (see Hall et al. 2017 for details). GLI has been used to evaluate and model the effect of forest management on canopy structure (Beaudet and Messier 2002; Drever and Lertzman 2003), and to predict seedling growth and morphology (Paquette et al. 2007b). It is used extensively in forest ecology research (e.g., Canham et al. 1990; Rich et al. 1993; Easter and Spies 1994). The direct and diffuse components can also be assessed separately, for example, to test their respective effects on seedling growth (Paquette et al. 2007b) or to characterize the duration and frequency distribution of sunflecks (Canham et al. 1990).

A local analysis can be computed for a flat surface and, where required, for an inclined one (Ameztegui et al. 2012). In a mountainous landscape, it can also be combined with a digital elevation model to take topographic shading and reflection into account. Scattering within the canopy cannot be directly estimated from the images as it varies too greatly over time. It is therefore usually neglected in these kinds of analyses, which can be a source of error, especially when the Sun is low over the horizon (e.g., morning, evening, winter, high latitudes) and canopy scattering is large compared to transmittance. Accordingly, HP has been found to be less precise in estimating the radiation regime under dense canopies (below about 6% light transmission) than under more open canopies (Machado and Reich 1999; Paquette et al. 2007b; also see Sect. 2.8). Local analyses are essentially used to study small-scale structures and processes. Some examples are forest regeneration in canopy gaps, reaction of photosynthesis to variable light, patterns of ground vegetation, habitat studies for rare or invasive plant species, and intensive plantation forestry (Paquette et al. 2008; Martin et al. 2010; Zlatanov et al. 2013).

### 2.7.3 *Canopy Analysis*

Canopy analysis does not look at photographic images in and of themselves but only as samples of the tree stand (or, in some cases, a single tree). Interpretation is thus not performed on a point-by-point basis; rather, it is integrated over the entire canopy. The properties that are derived from this analysis typically include canopy openness, LAI, mean leaf angle, and a clumping factor (Bréda 2003). The information that is contained in one, or usually several photographs, is used to characterize the canopy. The radiation regime can then be evaluated indirectly, i.e., by combining the incident radiation with a canopy model (and no longer with the pictures themselves). Such analyses are often conducted with the objective of obtaining important input parameters for ecosystem (process) models (Boivin et al. 2011; Ameztegui et al. 2012). They apply to processes that act at the stand-level, such as forest productivity, forest hydrology and climate, and suitability as habitat for animal species (Dobbertin et al. 2010; Manetti et al. 2010).

## 2.8 Comparison of HP with Other Methods Used to Estimate Understory Light Availability in Forests

As stated in this chapter's Introduction (Sect. 2.1), understory light plays an important role in forest dynamics, especially for the survival and growth of tree seedlings. Over the years, researchers have developed techniques for evaluating understory light availability as accurately as possible. A standard and direct method is to assess the transmittance of PAR, sometimes called %PAR or %PPFD, over the whole growing season (hereafter, $T_{PAR}$). This involves continuous measurements at given locations in the understory (e.g., using quantum sensors). An additional sensor that is positioned above the canopy to record incident PAR is used as a reference for computing $T_{PAR}$ ratios (Comeau et al. 1998; Gendron et al. 1998). This method is simple in design and exhaustive in rendering the time variability. Nevertheless, it has limited use because it requires several sensors and data loggers over a long period of time (Rich et al. 1993; Machado and Reich 1999). A faster method is to measure the instantaneous transmittance under an overcast sky (Messier and Puttonen 1995; Parent and Messier 1996). It is fast, reliable, and has become a popular alternative in recent years; however, the overcast sky conditions that are required can be restrictive (Paquette et al. 2007b). HP is also fast but, for local analysis, it allows one to reconstruct how light transmission varies through time following the position of the Sun. We reviewed comparisons of direct PAR measurements with the gap light index (GLI, see Sect. 2.7.2) that was derived from hemispherical photographs (Table 2.2). For the different forest types that have been studied, GLI correlates well with most of the other available methods. It compares particularly well with the standard continuous measurement of $T_{PAR}$ over the growing season.

## 2.9 Conclusion

In this chapter, we have presented theoretical aspects that are important for the application of HP in forests. We examined how solar radiation interacts with the atmosphere, vegetation and soil, as well as how reflected and reemitted radiation behaves in this system. The concepts and physical laws that have been introduced will enable the reader to better understand the following chapters in this book. They clarify the relationships that exist within a hemispherical image, the structures of the canopy that it depicts, and the function of the canopy. In many cases, HP is a useful technique. Like all other measurements that are used to assess radiation in forests, it has both strengths and limitations. Its main strength is undoubtedly its ability to cover all directions of the hemisphere in one measurement. Spatial and temporal dimensions can be taken into account by taking additional photographs across space and time; however, the dimension of wavelength is not measured in a useful manner. The precision, accuracy, and repeatability of HP are limited compared to other instruments that are specifically designed to measure radiation. Depending upon the application, HP may therefore be used in conjunction with models or with other instruments.

**Acknowledgements** We thank William F.J. Parsons and Catherine A. Brown for editing the language of our manuscript.

## References

Aber JD, Federer CA (1992) A generalized, lumped-parameter model of photosynthesis, evapotranspiration and net primary production in temperate and boreal forest ecosystems. Oecologia 92:463–474

Akinoglu BG (2008) Recent advances in the relations between bright sunshine hours and solar irradiation. In: Badescu V (ed) Modeling solar radiation at the Earth surface, recent advances. Springer, Berlin, pp 115–143

Ameztegui A, Coll L, Benavides R, Valladares F, Paquette A (2012) Understory light predictions in mixed conifer mountain forests: role of aspect-induced variation in crown geometry and openness. For Ecol Manag 276:52–61

Anderson MC (1964) Studies of the woodland light climate I. The photographic computation of light condition. J Ecol 52:27–41

Angström A (1924) Solar and terrestrial radiation. Q J Roy Meteor Soc 50:121–126

Appelbaum J (1987) A solar radiation distribution sensor. Sol Energy 39:1–10

Ballaré CL (1999) Keeping up with the neighbours: phytochrome sensing and other signalling mechanisms. Trends Plant Sci 4:97–102

Battaglia MA, Mitchell RJ, Mou PP, Pecot SD (2003) Light transmittance estimates in a longleaf pine woodland. For Sci 49:752–762

Beaudet M, Messier C (2002) Variation in canopy openness and light transmission following selection cutting in northern hardwood stands: an assessment based on hemispherical photographs. Agric For Meteorol 110:217–228

Beaudet M, Messier C, Canham CD (2002) Predictions of understorey light conditions in northern hardwood forests following parameterization, sensitivity analysis, and tests of the SORTIE light model. For Ecol Manag 165:235–248

Berbigier P, Bonnefond JM (1995) Measurement and modelling of radiation transmission within a stand of maritime pine (*Pinus pinaster* Ait.). Ann Sci For 52:23–42

Bohren CF, Clothiaux EE (2006) Fundamentals of atmospheric radiation. Wiley-VCH, Weinheim

Boivin F, Paquette A, Racine P, Messier C (2011) A fast and reliable method for the delineation of tree crown outlines for the computation of crown openness values and other tree crown parameters. Can J For Res 41:1827–1835

Bonhomme R, Chartier P (1972) The interpretation and automatic measurement of hemispherical photographs to obtain sunlit foliage area and gap frequency. Israel J Agric Res 22:53–61

Borthwick HA, Hendricks SB, Parker MW, Toole EH, Toole VK (1952) A reversible photoreaction controlling seed germination. Proc Natl Acad Sci U S A 38:662–666

Brasseur F, de Sloover JR (1976) L'extinction du rayonnement dans les gammes spectrales bleu, rouge et rouge lointain. Comparaison de deux peuplements forestiers de Haute-Ardenne. Bull Soc R Bot Belg 109:319–334

Bréda NJJ (2003) Ground-based measurements of leaf area index: a review of methods, instruments and current controversies. J Exp Bot 54:2403–2417

Brunger AP, Hooper FC (1993) Anisotropic sky radiance model based on narrow field of view measurements of shortwave radiance. Sol Energy 51:53–64

Burch H, Forster F, Schleppi P (1996) Zum Einfluss des Waldes auf die Hydrologie der Flysch-Einzugsgebiete des Alptals. Schweiz Z Forstwes 147:925–938

Butler WL, Norris KH, Siegelman HW, Hendricks SB (1959) Detection, assay, and preliminary purification of the pigment controlling photoresponsive development of plants. Proc Natl Acad Sci U S A 45:1703–1708

Campbell GS (1986) Extinction coefficients for radiation in plant canopies calculated using an ellipsoidal inclination angle distribution. Agric For Meteorol 36:317–321

Canham CD (1988) An index for understory light levels in and around canopy gaps. Ecology 69:1634–1638

Canham CD, Denslow JS, Platt WJ, Runkle JR, Spies TA, White PS (1990) Light regimes beneath closed canopies and tree-fall gaps in temperate and tropical forests. Can J For Res 20:620–631

Canham CD, Coates KD, Bartemucci P, Quaglia S (1999) Measurement and modeling of spatially explicit variation in light transmission through interior cedar-hemlock forests of British Columbia. Can J For Res 29:1775–1783

Canham CD, Murphy LE (2005) SORTIE-ND. Cary Institute of Ecosystem Studies, Millbrook, New York. http://www.sortie-nd.org/

Chen JM, Cihlar J (1995) Plant canopy gap-size analysis theory for improving optical measurements of leaf-area index. Appl Opt 34:6211–6222

CIE (2003) Spatial distribution of daylight—CIE standard general sky (ISO 15469:2004 (E)/CIE S 011/E:2003). Commission Internationale de l'Éclairage, Vienna, Austria

Comeau PG, Gendron F, Letchford T (1998) A comparison of several methods for estimating light under a paper birch mixedwood stand. Can J For Res 28:1843–1850

Côté J-F, Widlowski J-L, Fournier RA, Verstraete MM (2009) The structural and radiative consistency of three-dimensional tree reconstructions from terrestrial lidar. Remote Sens Environ 113:1067–1081

Côté J-F, Fournier RA, Verstraete MM (2017) Canopy architectural models in support of methods using hemispherical photography. In: Fournier RA, Hall RJ (eds) Hemispherical photography in forest science: theory, methods, applications. Springer, Berlin

Dai Q, Sun S (2006) A generalized layered radiative transfer model in the vegetation canopy. Adv Atmos Sci 23:243–257

Dai Q, Sun S (2007) A comparison of two canopy radiative models in land surface processes. Adv Atmos Sci 24:421–434

de Pury DGG, Farquhar GD (1997) Simple scaling of photosynthesis from leaves to canopies without the errors of big-leaf models. Plant Cell Environ 20:537–557

Dickinson RE (1983) Land surface processes and climate—surface albedos and energy-balance. Adv Geophys 25:305–353
Dobbertin M, Eilmann B, Bleuler P, Giuggiola A, Pannatier EG, Landholt W, Schleppi P, Rigling A (2010) Effect of irrigation on needle morphology, shoot and stem growth in a drought-exposed *Pinus sylvestris* forest. Tree Physiol 30:346–360
Drever CR, Lertzman KP (2003) Effects of a wide gradient of retained tree structure on understory light in coastal Douglas-fir forests. Can J For Res 33:137–146
Easter MJ, Spies TA (1994) Using hemispherical photography for estimating photosynthetic photon flux density under canopies and in gaps in Douglas-fir forests of the Pacific Northwest. Can J For Res 24:2050–2058
Emery K, Myers D (2008) Reference solar spectral irradiance: air mass 1.5. http://rredc.nrel.gov/solar/spectra/am1.5. Accessed 5 Mar 2013
Engler A (1924) Heliotropismus und Geotropismus der Bäume und deren waldbauliche Bedeutung. Mitteilungen der Schweizerischen Zentralanstalt für das forstliche Versuchswesen 13:225–283
Endler JA (1993) The color of light in forests and its implications. Ecol Monogr 63:1–27
Essery R (1998) Boreal forests and snow in climate models. Hydrol Process 12:1561–1567
Evans GD, Coombe DE (1959) Hemispherical and woodland canopy photography and the light climate. J Ecol 47:103–113
Feldhake CM (2002) Forage frost protection potential of conifer silvopastures. Agric For Meteorol 112:123–130
Frazer GW, Fournier RA, Leblanc SG, Walter J-MN (2017) View angle-dependent clumping indices for indirect LAI estimation. In: Fournier RA, Hall RJ (eds) Hemispherical photography in forest science: theory, methods, applications. Springer, Berlin
Gates DM (1980) Biophysical ecology. Springer, Berlin
Geiger R, Aron RH, Todhunter P (2009) The climate near the ground, 7th edn. Rowman & Littlefield, Lanham
Gendron F, Messier C, Comeau PG (1998) Comparison of various methods for estimating the mean growing season percent photosynthetic photon flux density in forests. Agric For Meteorol 92:55–70
Goudriaan J (1977) Crop micrometeorology: a simulation study. Dissertation, Center for Agricultural Publishing and Documentation, University of Wageningen, Wageningen
Gower ST, Norman JM (1991) Rapid estimation of leaf area index in conifer and broad-leaf plantations. Ecology 72:1896–1900
Grant RH, Heisler GM, Gao W (1996) Photosynthetically-active radiation: sky radiance distributions under clear and overcast conditions. Agric For Meteorol 82:267–292
Hall RJ, Fournier RA, Côté J-F, Mailly D (2017) Comparison of software tools for analysis of hemispherical photography. In: Fournier RA, Hall RJ (eds) Hemispherical photography in forest science: theory, methods, applications. Springer, Berlin
Harrison AW, Coombes CA (1988) Angular distribution of clear sky short wavelength radiance. Sol Energy 40:57–63
Hawke MF, Wedderburn ME (1994) Microclimate changes under *Pinus radiata* agroforestry regimes in New Zealand. Agric For Meteorol 71:133–145
Hay JE, McKay DC (1985) Estimating solar irradiance on inclined surfaces: a review and assessment of methodologies. Int J Sol Energy 3:203–240
Hill R (1924) A lens for whole sky photographs. Q J R Meteorol Soc 50:227–235
Hooper FC, Brunger AP (1980) A model for the angular distribution of sky radiance. J Sol Energy-T ASME 102:196–202
Iqbal M (1983) An introduction to solar radiation. Academic Press, Toronto
Jacobson MZ (2002) Atmospheric pollution: history, science, and regulation. Cambridge University Press, Cambridge, p 399 pp
Jonckheere IGC, Macfarlane C, Walter J-MW (2017) Image Analysis of hemispherical photographs, algorithms and calculation. In: Fournier RA, Hall RJ (eds) Hemispherical photography in forest science: Theory, methods, applications. Springer, New York

Kittler R (1994) Some qualities of scattering functions defining sky radiance distributions. Sol Energy 53:511–516

Körner C (2007) Climatic treelines: conventions, global patterns, causes. Erdkunde 61:316–324

Kucharik CJ, Norman JM, Murdock LM, Gower ST (1997) Characterizing canopy nonrandomness with a multiband vegetation imager (MVI). J Geophys Res 102(D24):29455–29473

LaMalfa EM, Ryle R (2008) Differential snowpack accumulation and water dynamics in aspen and conifer communities: implications for water yield and ecosystem function. Ecosystems 11:569–581

Lang M, Kuusk A, Mõttus M, Rautiainen M, Nilson T (2010) Canopy gap fraction estimation from digital hemispherical images using sky radiance models and a linear conversion method. Agric For Meteorol 150:20–29

Langensiepen M, Burgess S, Lambers H, Mitchell P, Veneklass E (2006) A model for simulating transpiration of *Eucalyptus salmonophloia* trees. Physiol Plant 127:465–477

Leblanc SG, Fournier RA (2014) Hemispherical photography simulations with an architectural model to assess retrieval of leaf area index. Agric For Meteorol 194:64–76

Leblanc SG, Fournier RA (2017) Measurement of forest structure with hemispherical photography. In: Fournier RA, Hall RJ (eds) Hemispherical photography in forest science: theory, methods, applications. Springer, Berlin

Leblanc SG, Chen JM, Fernandes R, Deering DW, Conley A (2005) Methodology comparison for canopy structure parameters extraction from digital hemispherical photography in boreal forests. Agric For Meteorol 129:187–207

Lemmon PE (1956) A spherical densiometer for estimating forest overstory density. For Sci 2:314–320

Lieffers VJ, Messier C, Stadt KJ, Gendron F, Comeau PG (1999) Predicting and managing light in the understory of boreal forests. Can J For Res 29:796–811

Liu BYH, Jordan RC (1961) Daily insolation on surfaces tilted towards the equator. Trans ASHRAE 67:526–541

Lodish H, Berk A, Zipursky SL, Matsudaira P, Baltimore D, Darnell J (2000) Molecular cell biology, 4th edn. Freeman, New York

Machado J-L, Reich PB (1999) Evaluation of several measures of canopy openness as predictors of photosynthetic photon flux density in deeply shaded conifer-dominated forest understory. Can J For Res 29:1438–1444

Manetti MC, Amorini E, Becagli C, Pelleri F, Pividori M, Schleppi P, Zingg A, Conedara M (2010) Quality wood production from chestnut (Castanea sativa Mill.) coppice forests—comparison between different silvicultural approaches. Acta Hortic 866:683–692

Martin PH, Canham CD, Kobe RK (2010) Divergence from the growth-survival trade-off and extreme high growth rates drive patterns of exotic tree invasions in closed-canopy forests. J Ecol 98:778–789

McCree KJ (1972) Test of current definitions of photosynthetically active radiation against leaf photosynthesis data. Agric For Meteorol 10:443–453

Messier C, Puttonen P (1995) Spatial and temporal variation in the light environment of developing Scots pine stands: the basis for a quick and efficient method of characterizing light. Can J For Res 25:343–354

Milankovitch M (1941) Kanon der Erdbestrahlungen und seine Anwendung auf das Eiszeitenproblem. Königlich Serbische Akademie, Belgrad

Montes F, Rubio A, Barbeito I, Cañellas I (2008) Characterization of the spatial structure of the canopy in *Pinus silvestris* L. stands in Central Spain from hemispherical photographs. For Ecol Manag 255:580–590

Myneni RB (1991) Modeling radiative transfer and photosynthesis in three-dimensional vegetation canopies. Agric For Meteorol 55:323–344

Norman JM (1982) Simulation of microclimates. In: Hatfield JL, Thomason IJ (eds) Biometeorology in integrated pest management. Academic Press, New York, pp 65–99

Pacala SW, Canham CD, Saponara J, Silander JA Jr, Kobe RK, Ribbens E (1996) Forest models defined by field measurements: estimation, error analysis and dynamics. Ecol Monogr 66:1–43

Paquette A, Bouchard A, Cogliastro A (2006) Survival and growth of under-planted trees: a meta-analysis across four biomes. Ecol Appl 16:1575–1589

Paquette A, Bouchard A, Cogliastro A (2007a) Morphological plasticity in seedlings of three deciduous species under shelterwood under-planting management does not correspond to shade tolerance ranks. For Ecol Manag 241:278–287

Paquette A, Bouchard A, Cogliastro A (2007b) A less restrictive technique for the estimation of understory light under variable weather conditions. For Ecol Manag 242:800–804

Paquette A, Messier C, Périnet P, Cogliastro A (2008) Simulating light availability under different hybrid poplar clones in a mixed intensive plantation system. For Sci 54:481–489

Paquette A, Fontaine B, Messier C, Brisson J (2010) Homogeneous light regime in shade-house experiment overestimates carbon gains in Norway maple seedlings. J Hortic For 2:117–121

Parent S, Messier C (1996) A simple and efficient method to estimate microsite light availability under a forest canopy. Can J For Res 26:151–154

Pearcy RW (1989) Radiation and light measurements. In: Pearcy RW, Ehleringer J, Mooney HA, Rundel PW (eds) Plant physiological ecology: field methods and instrumentation. Chapman & Hall, New York, pp 95–116

Pelkowski J (2008) Insolation at the Earth's surface. Rev Acad Colomb Ci Exact 32:25–35

Porté A, Bosc A, Champion I, Loustau D (2000) Estimating the foliage area of maritime pine (*Pinus pinaster* Ait.) branches and crowns with application to modelling the foliage area distribution in the crown. Ann For Sci 57:73–86

Posada JM, Lechowicz MJ, Kitajima K (2009) Optimal photosynthetic use of light by tropical tree crowns achieved by adjustment of individual leaf angles and nitrogen content. Ann Bot 103:795–805

Prescott JA (1940) Evaporation from a water surface in relation to solar radiation. Trans R Soc South Aust 64:114–116

Renaud V, Rebetez M (2009) Comparison between open-site and below-canopy climatic conditions in Switzerland during the exceptionally hot summer of 2003. Agric For Meteorol 149:873–880

Rich PM (1990) Characterizing plant canopies with hemispherical photographs. In: Goel NS, Norman JM (eds) Instrumentation for studying vegetation canopies for remote sensing in optical and thermal infrared regions. Remote Sens Rev 5:13–29

Rich PM, Clark DB, Clark DA, Oberbauer SF (1993) Long-term study of solar radiation regimes in a tropical wet forest using quantum sensors and hemispherical photography. Agric For Meteorol 65:107–127

Ross J (1981) The radiation regime and architecture of plant stands. Dr W. Junk publishers, The Hague

Roussel L (1972) Photologie forestière. Masson, Paris, p 144 pp

Running SW, Coughlan JC (1988) A general model of forest ecosystem processes for regional applications. I. Hydrologic balance, canopy gas-exchange and primary production processes. Ecol Model 42:125–154

Schleppi P, Conedera M, Sedivy I, Thimonier A (2007) Correcting non-linearity and slope effects in the estimation of the leaf area index of forests from hemispherical photographs. Agric For Meteorol 144:236–242

Schütz J, Brang P (1995) L'horizontoscope: un étonnant outil pratique de sylviculture, notamment en haute montagne. Office National des Forêts, Bulletin Technique 28

Sellers PJ (1985) Canopy reflectance, photosynthesis and transpiration. Int J Remote Sens 6:1335–1372

Sellers PJ, Berry JA, Collatz GJ, Field CB, Hall FG (1992) Canopy reflectance, photosynthesis, and transpiration. III. A reanalysis using improved leaf models and a new canopy integration scheme. Remote Sens Environ 42:187–216

Siala FMF, Hooper FC (1990) A model for the directional distribution of the diffusive sky radiance with an application to a CPC collector. Sol Energy 44:291–296

Sinclair TR, Murphy CE Jr, Knoerr KR (1976) Development and evaluation of simplified models for simulating canopy photosynthesis and transpiration. J Appl Ecol 13:813–829

Singhal GS, Renger G, Sopory SK, Irrgang KD, Govindjee (eds) (1999) Concepts in photobiology: photosynthesis and photomorphogenesis. Narosa Publishing House, New Delhi, p 1019 pp

Smith WK, Knapp AK, Reiners WA (1989) Penumbral effects on sunlight penetration in plant communities. Ecology 70:1603–1609

Smolander S (1984) Measurement of fluctuating irradiance in field studies of photosynthesis. Acta For Fenn 187:1–56

Smolander S, Stenberg P (2005) Simple parameterizations of the radiation budget of uniform broadleaved and coniferous canopies. Remote Sens Environ 94:355–363

Spencer JW (1971) Fourier series representation of the position of the Sun. Search 2:172

Stähli M, Jonas T, Gustafsson D (2009) The role of snow interception in winter-time radiation processes of a coniferous sub-alpine forest. Hydrol Process 23:2498–2512

Stanhill G (1970) Some results of helicopter measurements of the albedo of different land surfaces. Sol Energy 13:59–66

Steven MD, Unsworth MH (1980) The angular distribution and interception of diffuse solar radiation below overcast skies. Q J R Meteorol Soc 106:57–61

Thimonier A, Sedivy I, Schleppi P (2010) Estimating leaf area index in different types of mature forest stands in Switzerland: a comparison of methods. Eur J For Res 129:543–562

Timofeyev YM, Vasil'ev AV (2008) Theoretical fundamentals of atmospheric optics. CABI, Cambridge

Torres JL, Torres LM (2008) Angular distribution of sky diffuse radiance and luminance. In: Badescu V (ed) Modeling solar radiation at the Earth's surface: recent advances. Springer, Berlin, pp 427–448

Tucker CJ (1979) Red and photographic infrared linear combinations for monitoring vegetation. Remote Sens Environ 8:127–150

Vida J, Foyo-Moreno I, Alados-Arboledas L (1999) Performance validation of MURAC, a cloudless sky radiance model proposal. Energy 24:705–721

Wang S, Chen W, Cihlar J (2002) New calculation methods of diurnal distribution of solar radiation and its interception by canopy over complex terrain. Ecol Model 155:191–204

Wang Q, Tenhunen J, Schmidt M, Otieno D, Kolcun O, Droesler M (2005) Diffuse PAR irradiance under clear skies in complex alpine terrain. Agric For Meteorol 128:1–15

Wang W-M, Li Z-L, Su H-B (2007) Comparison of leaf angle distribution functions: effects on extinction coefficient and fraction of sunlit foliage. Agric For Meteorol 143:106–122

Way DA, Pearcy RW (2012) Sunflecks in trees and forests: From photosynthetic physiology to global change biology. Tree Physiol 32:1066–1081

Zlatanov T, Schleppi P, Velichkov I, Hinkov G, Georgieva M, Eggertsson O, Zlatanova M, Vacik H (2013) Structural diversity of abandoned chestnut (*Castanea sativa* Mill.) dominated forests: Implications for forest management. For Ecol Manag 291:326–335